Performance optimization of c-Si solar cell by tuning the device parameters

A thesis submitted in partial fulfillment of the requirements for the degree of Master of Science in Renewable Energy Technology

Institute of Energy, University of Dhaka

By

Examination Roll number: 404
Registration number: Ha 309
Admission session: 2013 - 2014

February 2016

Supervisor's Declaration

The MS level research on "Performance optimization of c-Si solar cell by tuning the device parameters" has been carried out and the dissertation was prepared under my direct supervision. Hereby I confirm that, to the best of my knowledge the thesis represents the original research work of the candidate; the contribution made to the research by me, by others of the University was consistent with normal supervisory practice, and external contributions to the research are acknowledged.

I believe the thesis to be in a suitable presentational form and is ready for examination.

Date: _____

Dr. Himangshu Ranjan Ghosh
Lecturer
Institute of Energy, University of Dhaka
Dhaka, Bangladesh

Candidate's Declaration

I confirm that this thesis represents my own work; the contribution of any supervisors and others to the research and to the thesis was consistent with normal supervisory practice. External contributions to the research are acknowledged.

Date: _____

Mirza Rakibul Hasan
MS student
3rd Semester, Admission Session 2013-2014
Institute of Energy, University of Dhaka
Dhaka, Bangladesh

Acknowledgement

The author wishes to express his deepest gratitude to his supervisor Dr. Himangshu Ranjan Ghosh for his guidance, advice, criticism, encouragements and insight throughout the research.

The author would also like to thank Prof. Dr. Saiful Huque, Director, The Institute of Energy, University of Dhaka, for his suggestions and comments and for providing proper research environment.

The PC1D software development team, University of New South Wales, Australia, is gratefully acknowledged. The technical assistance of Mazhar Kibria Parash, assistant manager, Seastar Shipping Lines Limited and Sirazum Munir, student of electrical & electronics engineering, Stamford University Bangladesh are also gratefully acknowledged.

Abstract

The performance of a solar cell depends upon different parameters of it. To study the effect of different parameters on the efficiency, different solar cell simulation software are well practiced in the advanced semiconductor research labs to skip repeated costly and time consuming experiments. A study utilizing the PC1D solar cell simulation software shows that a crystalline silicon solar cell gives optimum performance having a very thin top n layer with total cell thickness of 80 μm, Surface texturing angle of 61^0, Back Surface Field (p^{++}) of about 95×10^{16} cm^{-3} more than the p layer, Anti reflection coating of MnO_2. The 86.4nm thick ARC layer with refractive index of 1.7355 showed a better internal and external quantum efficiency at the visible range of solar spectrum with around 92% EQE at 600nm light wavelength. The research reveals that overall efficiency improvement of 5.5% is possible for proper selection of dimension, electrical and optical parameters of the c-Si solar cell.

Table of Contents

List of Tables

List of Figures

Glossary

A	Cross sectional area of p-n diode
APCVD	Atmospheric Pressure Chemical Vapor Deposition
ARC	Anti Reflection Coating
BSF	Back Surface Field
CVD	Chemical Vapor Deposition
D_e	Electron diffusion coefficient
D_h	Hole diffusion coefficient
D_n	Electron diffusivity
D_p	Hole diffusivity
E_g	Band Gap
G_{th}	Carrier Generation Rate
h	Plank‘s Constant
I_D	Junction Current Flow
I_L	Load Current
I_o	Reverse saturation current (dark current)
I_R	Light Generated Current
I_{sc}	Short Circuit current
J	Current Density
J_{cond}	Total Conduction Current Density
J_{dark}	Dark or Saturation Current Density
J_m	Current Density at Maximum Power
J_n	Total Current Density for Electrons
J_p	Total Current Density for Holes
K	Boltzmann constant

L_e	Minority carrier diffusion length for electron
L_h	Minority carrier diffusion length for hole
n	Density of Free Electrons
N_A	Acceptor densities
N_D	Donar densities
n_i	Intrinsic Carrier Concentration
n_{no}	Electron Densities in an n-type Semiconductor at Thermal Equilibrium
n_{no}	Electron density
N_{st}	Recombination Center density per Unit Area in the surface region
N_t	Concentration of the Recombination Center in the Semiconductor
p	Density of Free Holes
P_d	Power Density
PECVD	Plasma Enhanced Chemical Vapor Deposition
P_{max}	Maximum Power Output
p_{no}	Holes Densities in an n-type Semiconductor at Thermal Equilibrium
p_{no}	Hole Density
P_s	Hole Concentrations at the Surface
q	Electronic charge
R	The rate of Direct Recombination
r_{ar}	Refractive Index of Coating Material
R_{aug}	The rate of Augur Recombination
R_L	Load Resistance
r_o	Refractive Index of Air
r_{sc}	Refractive Index of Silicon
R_{th}	Carrier Recombination Rate
SEM	Scanning Electron Microscope

S_{lr}	Surface recombination Velocity
SRV	Surface recombination Velocity
T	Temperature
U	The rate of Indirect Recombination
V	Junction Imposed Voltage
V_L	Load Voltage
V_m	Voltage at Maximum Power
V_{oc}	Open Circuit Voltage
v_{th}	Thermal Velocity of Carriers
ε	Electric Field
λ_0	Free Space Wavelength
σ_n	The Capture Cross Section of Electrons
σ_p	The Capture Cross Section of Holes
η	Efficiency
υ	Light Energy of Frequency
τ_p	Life time of Excess minority carrier
μ_n	Electron Mobility
μ_p	Hole Mobility

1 Introduction

The Sun is the ultimate source of energy. Indirect product of solar energy, i.e. coal and natural gas are utilized to produce conventional energies. The problem of these fossil fuels is that they can't be replaced - once one use them up, they're gone forever. Another problem is that fossil fuels can cause environmental pollutions.

Unlike fossil fuels, some non-conventional energies i.e. solar energy, wind energy can be replaced. These renewable energies are also called "clean energy" or "green power" because it doesn't pollute the air or the water. Photovoltaics is the process of converting sunlight directly into electricity using solar cells. Today it is a rapidly growing and increasingly important renewable alternative to conventional fossil fuel electricity generation.

1.1 Literature Survey

Crystalline silicon solar cells have dominated the photovoltaic market since the very beginning in the 1950's. Silicon is non-toxic and abundantly available in the earth crust, silicon PV modules have shown their long-term stability over decades in practice. The price reduction of silicon modules in the last 30 years can be described very well by a learning factor of 20%, i.e. doubling the cumulated module capacity results in a reduction of module prices by 20%. To extend the success story of this photovoltaic working horse, it is important to further bring down the costs.

The cost distribution of a crystalline silicon PV module is clearly dominated by material costs, especially by the costs of the silicon wafer. Therefore besides improved production technology, the efficiency of the cells and modules is the main leverage to bring down the costs even more.

In 1941 the first silicon solar cell was reported by Ohl et al. [1]. It featured a melt-grown pn- junction and an energy conversion efficiency of less than 1%. A large progress was then achieved in the early 1950ies where Pearson, Fuller and Chapin in the Bell Laboratories prepared silicon solar cells with a diffused pn-junction. The first cells were fabricated on p-type silicon and reached an efficiency up to around 4.5% [2]. Then they switched to arsenic-doped n type silicon with a boron-doped emitter [3]. This increased efficiency to a value of more than 6%. The first application for these "solar batteries" was

the power supply of satellites. It won the competition against other power supplies as chemical batteries [4]. The space race was of national interest for Americans and Soviets during the cold war and solar cells played an important technical role. In fact, today photovoltaic panels are still the dominant power source for satellites and other space applications. Up to the end of the 1950s the cells were mainly fabricated on n-type silicon leading to superior efficiencies up to around 14%. However it was found that space radiation hardness was less detrimental for cells with a p-type base [5]. This was getting even clearer when a high-atmosphere nuclear bomb was ignited by the Americans leading to failure of the solar panels of satellites [6]. Thus in the early 60ties there was a switch to cells on p-type silicon with a phosphorus-doped emitter [7]. These cells had a higher radiation hardness but started with a lower efficiency. It took up to 1973 to achieve higher efficiencies with cells on p-type silicon than those reached in the early 1960ies with cells on n-type base.

A second strong phase of cell development started in 1980s with the passivated emitter solar cell (PESC) clearing the important 20%-hurdle in 1985 [8]. The PESC1 cell and also its successors the PERC2 [9] and the PERL3 [10] solar cell have a very important feature in common: surface passivation in order to reduce recombination of charge carriers at the surfaces. Indeed this is a crucial prerequisite for all high-efficiency silicon solar cells particularly for interdigitated back-contact cells [11], [12] where the collecting junction is at the rear side and most carriers have to diffuse a long way. Back contact cells played always an important role in the race for record efficiencies and are the base structure for today's best commercial solar cells with efficiencies greater than 22%.The best efficiency for a monocrystalline silicon solar cell is 25% [2], [13] getting quite close to the "practical" limit of around 26% [14].

In 2008, the world annual production of photovoltaic (PV) cells reached more than 7.9 GW_p (W_p, peak power under standard test conditions) [15], and the average annual growth rate in PV cell production over the last decade has been more than 40%. Yet the electrical power generated by all PV systems around the world has been estimated to be less than 0.1% of the total world electricity generation [15]. Nevertheless, the strong growth in PV cell production is expected to continue for many years. Crystalline silicon PV cells, with over 60 years of development, have the longest production history and now account for the largest share of production, comprising up to 90% of all the solar cells produced in

2008[1]. Silicon is safe for the environment and one of the most abundant resources on Earth, representing 26% of crustal material. The abundance and safety of silicon as a resource grants the silicon solar cell a prominent position among all the various kinds of solar cells in the PV industry. World annual PV cell production of 100 GW_p is expected to be achieved by around 2020, and the silicon PV cell is the most viable candidate to meet this demand from the point of view of suitability for large-volume production.

Computer-based simulations play a critical role in the design, development, and functionality of solar cells. Device modeling techniques substantially reduce the time and costs through optimization of process steps, choice of materials, and wafers. In this study, solar cell devices have been modeled using actual physical device configurations. This research has focused on variation of different device parameters and study the effects on the variations on crystalline silicon solar cell efficiency using modern simulation software like PC1D [16] (Annexure 01).

1.2 Objectives

The overall objective of this thesis is to study the solar cell performance and design optimization by varying different parameter using PC1D software. In brief the objectives of the research were

1. To study the solar cell operation
2. To observe the solar cell performance by varying surface area
3. To observe the solar cell performance by varying thickness of n and p region
4. To observe the solar cell performance by varying the doping and thickness of BSF p++ layer in rear surface
5. To observe the solar cell performance by using different anti-reflection coating
6. To observe the solar cell performance by varying texture angle

1.3 Chapter Contents

The rest of the thesis is organized as follows.

Chapter 2 guides the reader about the solar cell. This chapter describes the structure and operation of the cell. The characteristics of the cell is also discussed.

Chapter 3 focuses on device parameters. This chapter describes the influences of the surface area, thickness of n and p layer. Different recombination processes are also described.

Chapter 4 describes antireflection coating and texturing. This chapter explains different methodologies of antireflection and texturing processes. The importance of antireflection and texturing are also described here.

Finally in **Chapter 5** the conclusions of the thesis are presented. Result for different parameters are shown here. At the end of the chapter some suggestion are presented for optimizing the cell efficiency.

2 PN Junction as Photo Voltaic Cell

A solar cell is an electronic device which directly converts sunlight into electricity. Light shining on the solar cell produces both a current and a voltage to generate electric power. This process requires firstly, a material in which the absorption of light raises an electron to a higher energy state, and secondly, the movement of this higher energy electron from the solar cell into an external circuit. The electron then dissipates its energy in the external circuit and returns to the solar cell. A variety of materials and processes can potentially satisfy the requirements for photovoltaic energy conversion, but in practice nearly all photovoltaic energy conversion uses semiconductor materials in the form of a *p-n* junction

2.1 Solar Cell Structure and Operation

A crystalline silicon solar cell is the material is altered so that one side is p-type, dominated by positive holes, and the other side is n-type, dominated by negative electrons. The pn junction is located so that the maximum light is absorbed near it. The free electrons and holes generated by light deep in the silicon diffuse to the pn junction and then separate to produce a current if the silicon is of sufficiently high quality.

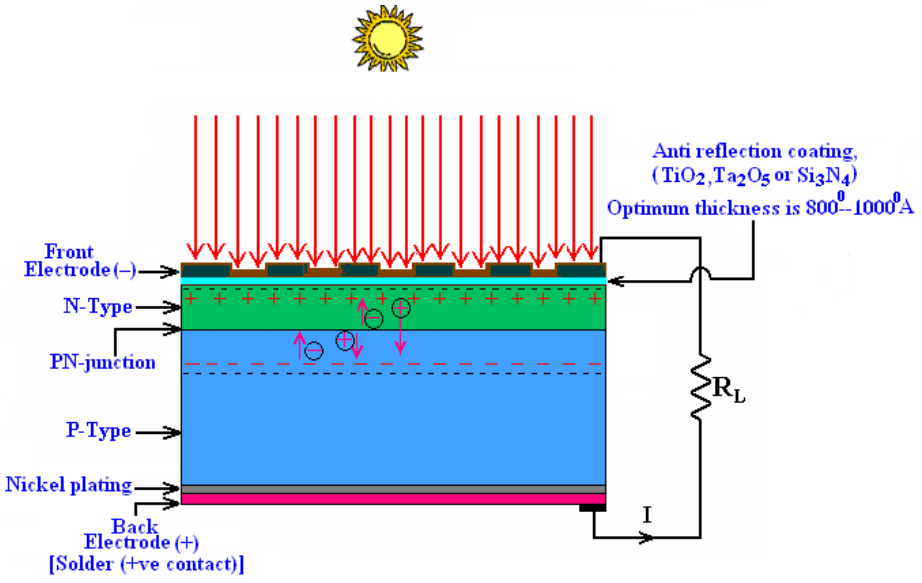

Figure 2-1 Cross section of silicon solar cell

The basic steps in the operation of a solar cell are:

- the generation of light-generated carriers;
- the collection of the light-generated carries to generate a current;

- the generation of a large voltage across the solar cell; and
- the dissipation of power in the load and in parasitic resistances.

When N-type and P-type materials are brought together in contact with each other forming a PN junction, the electron in the N type region, being very numerous, will diffuse into the P-type region giving rise to diffusion current. Similarly, holes from P-type region diffuse into the N-type region and both electrons and holes recombine. As a result, positive ions created near the junction edge in N-region, which are fixed at lattice point and are immobile. Similarly, holes from the P-region diffuse in the N-region creating negative ions in P-region near the junction edge.

If more holes try to diffuse across the junction, they are repelled by positive ions near the junction edge in the N-region. Similarly, the electrons from the N-region attempting to diffuse across the junction are repelled by negative ions in the P-region near the junction edge. Thus, an equilibrium condition is attained, which is represented in Fig.2-2 (a). Fig.2-2 (b) shows the potential profile in the depletion region and (c) indicates the carrier densities of N-type and P-type respectively.

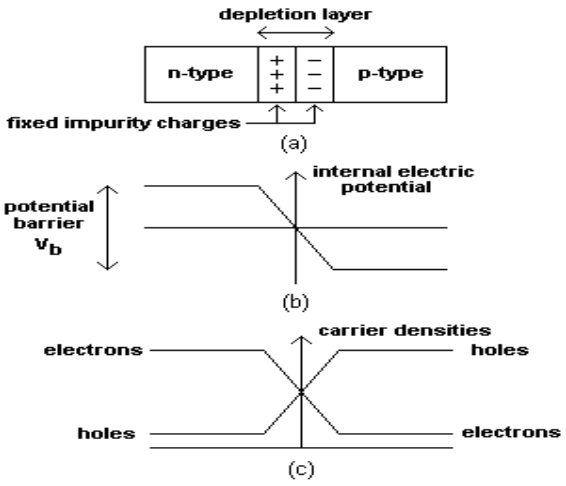

Figure 2-2 The structure of a semiconductor n-p junction

This accumulation of opposite charges on two sides of the junction results in the creation of an electric potential across it, known as potential barrier. The strength of the barrier potential depends on the substrate material and doping concentration. The region up to which the ionized immobile impurity ions are extended is called the depletion region as shown in Fig.2-3 (a). Fig.2-3 (b) and (c) show what happens to the band structure of P-

type and N-type materials and Fig.2-3 (d) represents the situation after the junction has been formed.

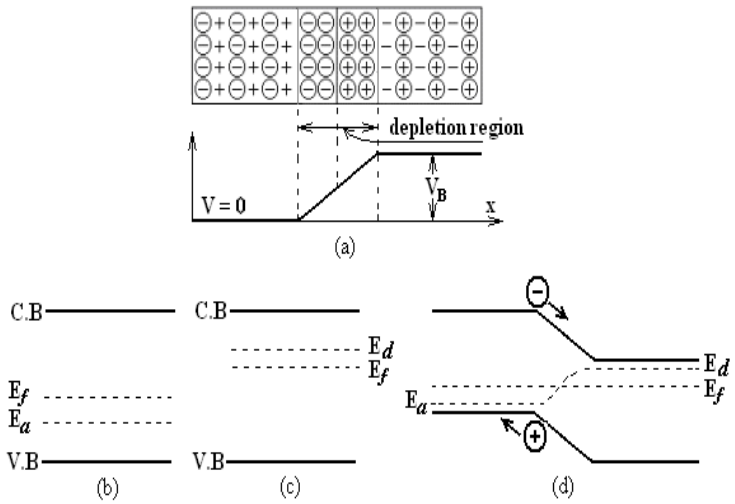

Figure 2-3 Energy Band diagrams of P-type, N-type and P-N junction

The highest filled electron energy at absolute zero is the Fermi-energy and the Fermi level must remain constant across the interface region since it must have the same value everywhere in the device. This means that in order to accommodate the band structure of the P-type material on the left and N-type material on the right, the band must be bent in a manner shown in Fig. 2-3 (d).

The equation that applies to the PN-junction for the relationship between the junction current flow, I_D and imposed voltage V , is

$$I_D = I_o \left(e^{\frac{q V_L}{kT}} - 1\right) \ldots\ldots\ldots\ldots\ldots\ldots\ldots\ldots\ldots\ldots \quad (2\text{-}1)$$

Where

I_0 = Reverse saturation current (sometimes called dark current)

q = Electronic charge

k = Boltzmann constant

T = Temperature

This relationship is sometimes shown schematically as curve-1 in Fig.2-4 (a). The saturation current I_0 is obtained when a large negative voltage is applied across the diode. When light energy of frequency υ such that $h\upsilon \geq E_g$ (where $h =$ Plank's constant and $E_g =$ band gap) is applied on the junction itself turns into a voltage source or generator of electric power. The minority carrier generated by the absorption of photons cross over the junction by diffusion in the negative direction of the concentration gradient. Fig.2-4

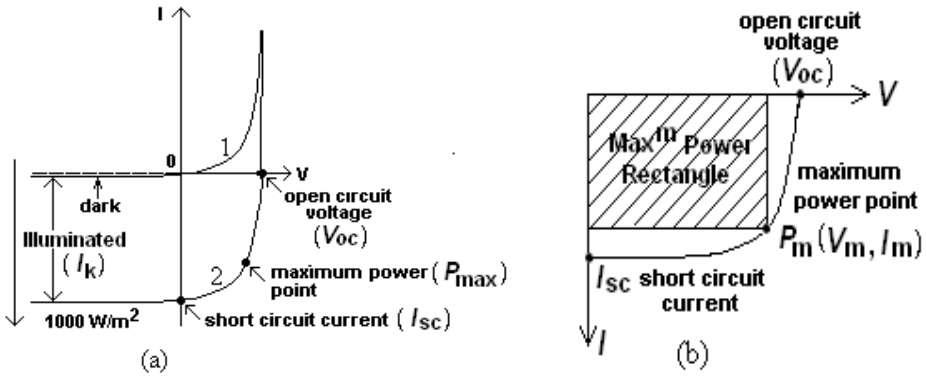

Figure 2-4 Current-voltage characteristics of (a) photovoltaic solar cell. (b) Maximum Power rectangle

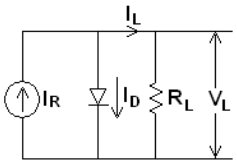

Figure 2-5 Equivalent Circuit of a solar cell

2.2 Ideal Characteristics of Solar Cell

2.2.1 Voltage and Current

Two important quantities to characterize a solar cell are

- Open circuit voltage (V_{oc}): The voltage between the terminals when no current is drawn (infinite load resistance)
- Short circuit current (I_{sc}): The current when the terminals are connected to each other (zero load resistance)

The short circuit current increases with light intensity, as higher intensity means more photons, which in turn means more electrons. Since the short circuit current I_{sc} is roughly proportional to the area of the solar cell, the short circuit current density, $J_{sc} = I_{sc}/A$, is often used to compare solar cells.

When a load is connected to the solar cell, the current decreases and a voltage develops as charge builds up at the terminals. The resulting current can be viewed as a superposition of the short circuit current, caused by the absorption of photons, and a dark current, which is caused by the potential built up over the load and flows in the opposite direction. As a solar cell contains a PN-junction (LINK), just as a diode, it may be treated as a diode. For an ideal diode, the dark current density is given by

$$J_{dark}(V) = J_o(e^{\frac{qV}{kT}} - 1) \quad \text{(2-2)}$$

Where,

J_o = Constant

q = Electronic charge

k = Boltzmann constant

T = Temperature

The resulting current can be approximated as a superposition of the short circuit current and the dark current:

$$J = J_{sc} - J_o(e^{\frac{qV}{kT}} - 1) \text{ .....} \quad (2\text{-}3)$$

To find an expression for the open circuit voltage, V_{oc}, we use (2-3) setting J = 0. This means that the two currents cancel out so that no current flows, which exactly is the case in an open circuit. The resulting expression is

$$V_{oc} = \frac{kT}{q} \ln(\frac{J_{sc}}{J_o} + 1) \text{.....} \quad (2\text{-}4)$$

2.2.2 Efficiency and Fill Factor

In general, the power delivered from a power source is P = IV, i.e. the product of voltage and current. If we instead use the current density J, we get the power density:

$$P_d = JV \text{ .....} \quad (2\text{-}5)$$

The maximum power density occurs somewhere between V = 0 (short circuit) and V = V_{oc} (open circuit) at a voltage V_m. The corresponding current density is called J_m, and thus the maximum power density is $P_{d,m} = J_m V_m$.

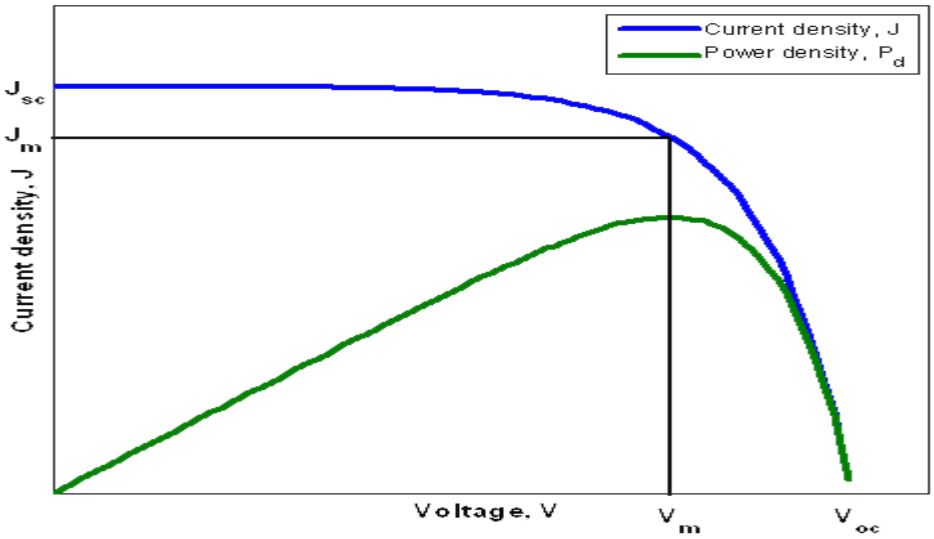

Figure 2-6 Maximum power

The efficiency of a solar cell is defined as the power (density) output divided by the power (density) output. If the incoming light has a power density P_s, the efficiency will be

$$\eta = \frac{J_m V_m}{P_s} \quad \text{..... (2-6)}$$

The fill factor, FF, is another quantity which is used to characterize a solar cell. It is defined as

$$FF = \frac{J_m V_m}{J_{sc} V_{oc}} \quad \text{..... (2-7)}$$

and gives a measure of how much of the open circuit voltage and short circuit current is "utilized" at maximum power. Using FF we can express the efficiency as

$$\eta = \frac{J_{oc} V_{oc} FF}{P_s} \quad \text{..... (2-8)}$$

The four quantities J_{sc}, V_{oc}, FF and η are frequently used to characterize the performance of a solar cell. They are often measured under standard lighting conditions, which implies Air Mass 1.5 spectrum, light flux of 1000W/m^2 and temperature of 25°C.

3 Device Parameter Optimization

A way of exploiting the solar energy is to use cells photovoltaic which convert the energy conveyed by the incident radiation in a continuous electric current. This conversion is based on the photovoltaic effect engendered by the absorption of photons. A part of the absorbed photons generates electron-hole pairs in which an electric field created in the zone of load of space of a junction p-n. Thus, the junction p-n, its characteristics, its component and its dimensions are the parameters responsible of the efficiency of a solar cell.

3.1 The effect of the surface area on the efficiency

The short circuit current I_{sc} is roughly proportional to the area of the solar cell (2.2.1). If the surface area of a solar cell increase, more photon will be absorbed & more current will be produced. Solar cell efficiency is the ratio of the electrical output of a solar cell to the incident energy in the form of sunlight. The energy conversion efficiency (η) of a solar cell is the percentage of the solar energy to which the cell is exposed that is converted into electrical energy. This is calculated by dividing a cell's power output (in watts) at its maximum power point (P_m) by the irradiance (input light), G, in W/m^2 and the surface area of the solar cell (A_c in m^2).

$$\eta = \frac{P_m}{G \times A_c} \quad \text{.....(3-1)}$$

The expression for the diode saturation current density I_o is given by,

$$I_o = qA\left(\frac{D_e n_i^2}{L_e N_A} + \frac{D_h n_i^2}{L_h N_D}\right) \quad \text{.....(3-2)}$$

Where,

q = Electron charge

A = Cross sectional area of p-n diode

D_e = Electron diffusion coefficient

D_h = Hole diffusion coefficient

L_e = Minority carrier diffusion length for electron

L_h = Minority carrier diffusion length for hole

n_i = The number of electron- hole pair

N_A = Acceptor densities

N_D = Donar densities

3.2 The effect of the thickness p and n layer on the efficiency

Due to general photovoltaic theory; light generated photocurrent (short circuit current) directly related to the created electron-hole pair number and it is well known that created e-h pairs directly related with captured number of photons. This process runs in the depletion width of the pn junction. During the solar cell fabrication n-type material is chosen from large band –gap semiconductor materials (window layer) and p-type material is chosen from lower band–gap semiconductor materials (absorber layer). Because all photons should be collected into depletion layer. Therefore, window layer (n-type semiconductor) should be transparent to let all photons have to move thoughts the p layer. Strong absorption occurs in the absorption layer. On the other hand number of photons roughly equals to light intensity. In addition, penetration depth of the light intensity in n or p type materials obeys the Beer–Lambert law. If there is demand of more photocurrent, semiconductor material should be kept as thinner as possible. According to beer lamberts law penetration depth of the material is directly related to absorption coefficient and band gap of the materials.

Since electron mobility is greater (roughly 3 times) than hole mobility, designers prefer to have p layer thicker than n layer so that the equal number of charge carriers (electron and hole) could reach at the opposite electrodes in almost equal time without getting recombined.

3.3 The effect of the generation and recombination on the efficiency [17]

In order to collect all of the light-generated carriers for the *p-n* junction, both surface and bulk recombinations must be minimized.

3.3.1 Generation and Recombination Process

In silicon solar cells, the two conditions commonly required for such current collection are:

- The carrier must be generated within a diffusion length of the junction, so that it will be able to diffuse to the junction before recombination; and
- In the case of a localized high recombination site (such as at an un passivated surface or at a grain boundary in multi crystalline devices), the carrier must be generated closer to the junction than to the recombination site. For less severe localized recombination sites, (such as a passivated surface), carriers can be generated closer to the recombination site while still being able to diffuse to the junction and be collected without recombination.

The presence of localized recombination sites at both the front and the rear surfaces of a silicon solar cell means that photons of different energy will have different collection probabilities. Since blue light has a high absorption coefficient and is absorbed very close to the front surface, it is not likely to generate minority carriers that can be collected by the junction if the front surface is a site of high recombination. Similarly, a high rear surface recombination will primarily affect carriers generated by infrared light, which can generate carriers deep in the device. The quantum efficiency of a solar cell quantifies the effect of recombination on the light generation current. The quantum efficiency of a silicon solar cell is shown below.

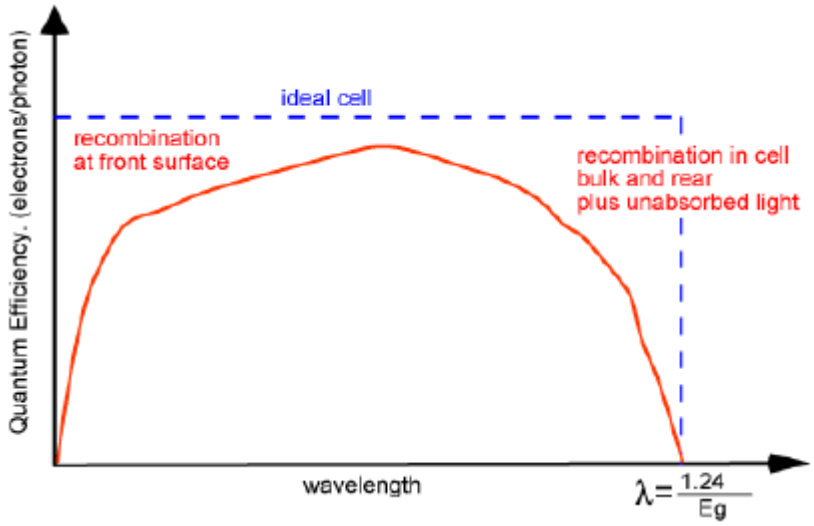

Figure 3-1 Typical quantum efficiency in an ideal and actual solar cell , illustrating the impact of optical and recombination losses

When an electric field is present in addition to a concentration gradient, both drift current and diffusion current will flow. The total current density at any point is the sum of the drift and diffusion components:

$$J_n = q\mu_n n\varepsilon + qD_n \frac{dn}{dx} \quad \text{.....(3-3a)}$$

Where,

ε = Electric field in the x-direction.

q = Eletronic charge

μ_n = Electron mobility

n = Density of free electrons

D_n = Electron diffusivity

A similar expression can be obtained for the hole current:

$$J_p = q\mu_p n\varepsilon + qD_n \frac{dp}{dx} \quad \text{.....(3-3b)}$$

Where,

ε = Electric field in the x-direction.

q = Eletronic charge

μ_p = Hole mobility

p = Density of free holes

D_p = Hole diffusivity

We use the negative sign in Eq. 3-3b because for a positive hole gradient the holes will diffuse in the negative x-direction. This diffusion results in a hole current that also flows in the negative x-direction.

The total conduction current density is given by the sum of Eqs. 3-3a and 3-3b:

$$J_{cond} = J_n + J_p \quad \text{.....(3-3c)}$$

The three expressions (Eqs. 3-3a-3-3c) constitute the current density equations. These equations are important for analyzing device operations under low electric fields.

In thermal equilibrium the relationship $pn=n_i^2$ is valid.

Where,

p = Density of free holes

n = Density of free electrons

n_i = Intrinsic carrier concentration

If excess carriers are introduced to a semiconductor so that $pn>n^2$, we have a non-equilibrium situation. The process of introducing excess carriers is called carrier injection. Most semiconductor devices operate by the creation of charge carriers in excess of the thermal equilibrium values. We can introduce excess carriers by optical excitation or forward-biasing a p-n junction

Whenever the thermal-equilibrium condition is disturbed (i.e., $pn \neq n_i^2$) processes exist to restore the system to equilibrium (i.e., $pn=n_i^2$). In the case of the injection of excess carriers, the mechanism that restores equilibrium is recombination of the injected minority carriers with the majority carriers. Depending on the nature of the recombination process, the released energy that results from the recombination process can be emitted as a photon or dissipated as heat to the lattice. When a photon is emitted, the process is called radiative recombination; otherwise, it is called nonradioactive recombination.

Recombination phenomena can be classified as direct and indirect processes. Direct recombination, also called band-to-band recombination, usually dominates in direct bandgap semiconductors, such as gallium arsenide, whereas indirect recombination via bandgap recombination centers dominates indirect bandgap semiconductors, such as silicon.

3.3.1.1 Direct recombination

Consider a direct-bandgap semiconductor in thermal equilibrium. The continuous thermal vibration of lattice atoms causes some bonds between neighboring atoms to be broken. When a bond is broken, an electron-hole pair is generated. In terms of the band diagram, the thermal energy enables a valence electron to make an upward transition to the

conduction band, leaving a hole in the valence band. This process is called carrier generation and is represented by the generation rate G_{th} (number of electron-hole pairs generated per cm^3 per second) in Fig. 3-2a. When an electron makes a transition downward from the conduction band to the valence band, an electron-hole pair is annihilated. This reverse process is called recombination; it is represented by the recombination rate R_{th} in Fig. 3-2a. Under thermal equilibrium conditions, the generation rate G_{th} must equal the recombination rate R_{th}, so that the carrier concentrations remain constant and the condition $pn = n_i^2$ is maintained.

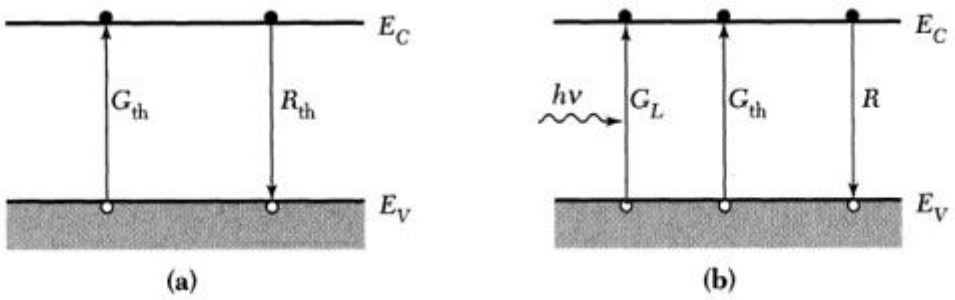

Figure 3-2 Direct generation and recombination of electron-hole pairs: (a) at thermal equilibrium and (b) under illumination

When excess carriers are introduced to a direct-bandgap semiconductor, the probability is high that electrons and holes will recombine directly, because the bottom of the conduction band and the top of the valence band are lined up and no additional momentum is required for the transition across the bandgap. The rate of the direct recombination R is expected to be proportional to the number of electrons available in the conduction band and the number of holes available in the valence band; that is,

$$R = \beta np \quad \text{.....(3-4)}$$

Where,

β = Proportionality constant

As discussed previously, in thermal equilibrium the recombination rate must be balanced by the generation rate. Therefore, for an n type semiconductor, we have,

$$G_{th} = R_{th} = \beta\, n_{no}\, p_{no} \quad \text{.....(3-5)}$$

Where,

n_{no} = electron densities in an n-type semiconductor at thermal equilibrium

p_{no} = hole densities in an n-type semiconductor at thermal equilibrium

When we shine a light on the semiconductor to produce electron-hole pairs at a rate G_L (Fig.3-2b), the carrier concentrations are above their equilibrium values. The recombination and generation rate become

$$R = \beta\, n_n\, p_n = \beta\, (n_{no} + \Delta n)\, (p_{no} + \Delta p) \quad \text{.....(3-6)}$$

$$G = G_L + G_{th} \quad \text{.....(3-7)}$$

where Δn and Δp are the excess carrier concentrations, given by

$$\Delta n = n_n - n_{no} \quad \text{.....(3-8a)}$$

$$\Delta p = p_n - p_{no} \quad \text{.....(3-8b)}$$

and Δn = Δp to maintain overall charge neutrality.

The net rate of change of hole concentration is given by

$$\frac{dp_n}{dt} = G - R = G_L + G_{th} - R \quad \text{.....(3-9)}$$

In steady state, $dp_n / dt = 0$. From Eq. 3-9 we have

$$G_L = R - G_{th} \equiv U \quad \text{.....(3-10)}$$

Where,

U = The net recombination rate.

Substituting Eqs.3-5 and 3-6 into Eq. 3-10 yields

$$U = \beta(n_{no} + p_{no} + \Delta p)\Delta p \quad \text{.....(3-11)}$$

For low-level injection Δp, $p_{no} << n_{no}$, Eq. 3-11 is simplified to

$$U \cong \beta n_{no} \Delta p = \frac{p_n - p_{no}}{\frac{1}{\beta n_{no}}} \quad \text{.....(3-12)}$$

Therefore, the net recombination rate is proportional to excess minority carrier concentration. Obviously, U = 0 in thermal equilibrium. The proportionality constant $1/\beta n_{np}$, is called the lifetime τ_p of the excess minority carriers, or

$$U \equiv \frac{p_n - p_{no}}{\tau_p} \quad \text{.....(3-13)}$$

Where,

$$\tau_p \equiv \frac{1}{\beta n_{no}} \quad \text{.....(3-14)}$$

The physical meaning of lifetime can best be illustrated by the transient response of a device after the sudden removal of the light source. Consider an n-type sample, as shown in Fig. 3-3a, that is illuminated with light and in which the electron-hole pairs are generated uniformly throughout the sample with a generation rate G_L. The time-dependent expression is given by Eq. 39. In steady state, from Eqs. 3-10 and 3-13

$$G_L = U = \frac{p_n - p_{no}}{\tau_p} \quad \text{.....(3-15)}$$

or

$$p_n = p_{no} + \tau_p G_L \quad \text{.....(3-15a)}$$

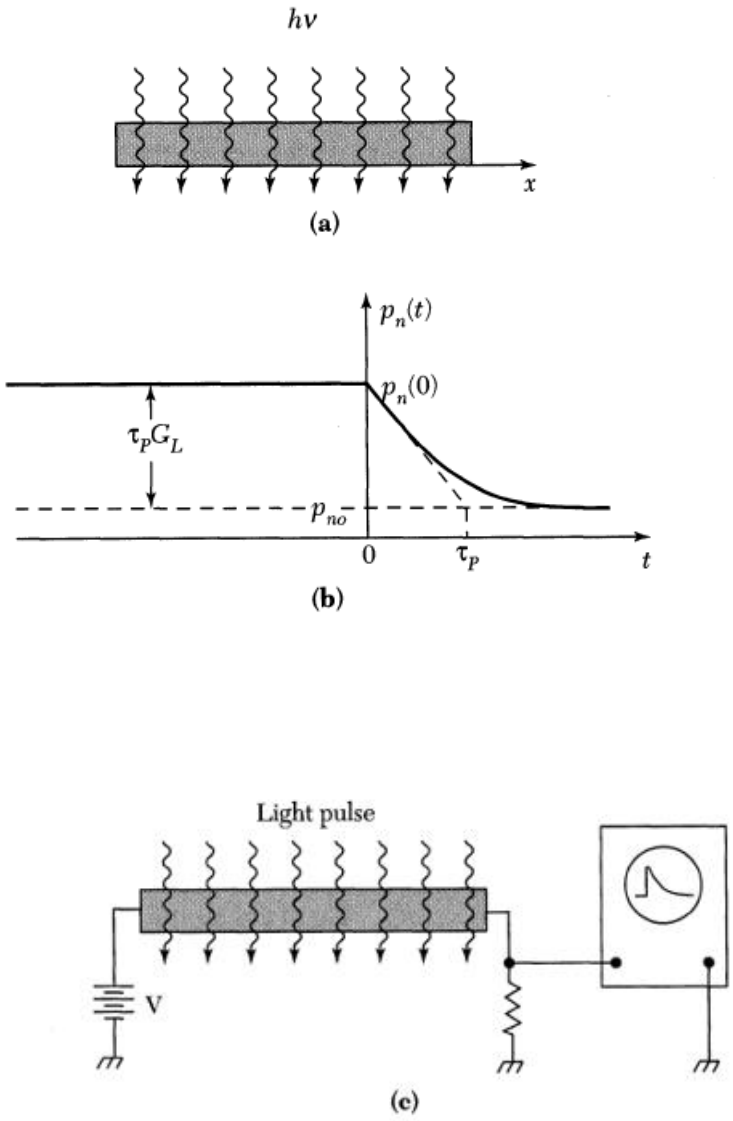

Figure 3-3 Decay of photo excited carriers. (a) n-type sample under constant illumination. (b) Decay of minority carriers (holes) with time. (c) Schematic setup to measure minority carrier lifetime

If at an arbitrary time, say $t = 0$, the light is suddenly turned off, the boundary conditions are $p,(t = 0) = p_{no} + G_L$, as given by Eq. 3-15a, and $p_n(\tau \rightarrow \infty) = p_{no}$. The time dependent expression of Eq. 3-9 becomes

$$\frac{dp_n}{dt} = G_{th} - R = -U = -\frac{p_n - p_{no}}{\tau_p} \quad \text{.....(3-16)}$$

and the solution is

$$p_n(t) = p_{no} + \tau_p G_L \exp(-t/\tau_p) \quad \text{.....(3-17)}$$

Figure 3-3b shows the variation of p_n with time. The minority carriers recombine with majority carriers and decay exponentially with a time constant τ_p, which corresponds to the lifetime defined in Eq. 3-14. This case illustrates the main idea of measuring the carrier lifetime using the photo conductivity method. Figure 3-3c shows a schematic setup. The excess carriers, generated uniformly throughout the sample by the light pulse, cause a momentary increase in the conductivity. The increase in conductivity manifests itself by a drop in voltage across the sample when a constant current is passed through it. The decay of the conductivity can be observed on an oscilloscope and is a measure of the lifetime of the excess minority carriers.

3.3.1.2 Indirect Recombination

For indirect-bandgap semiconductors, such as silicon, a direct recombination process is very unlikely, because the electrons at the bottom of the conduction band have nonzero momentum with respect to the holes at the top of the valence band. A direct transition that conserves both energy and momentum is not possible without a simultaneous lattice interaction. Therefore the dominant recombination process in such semiconductors is indirect transition via localized energy states in the forbidden energy gap. These states act as stepping stones between the conduction band and the valence band.

Figure 3-4 shows various transitions that occur in the recombination process through intermediate-level states (also called recombination centers). The arrows in the figure designate the transition of the electron in a particular process. The illustration is for the case of a recombination center with a single energy level that is neutral when not occupied by an electron or negative when it is occupied. In indirect recombination,

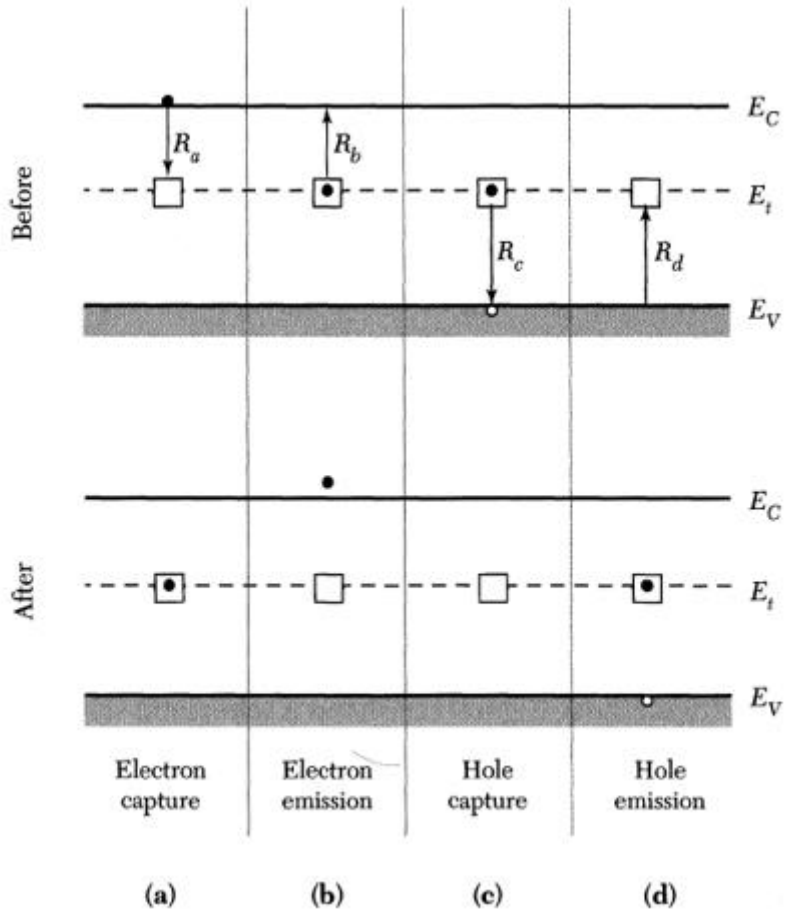

Figure 3-4 Indirect generation-recombination process at thermal equilibrium

The derivation of the recombination rate is more complicated. The recombination rate is given by

$$U = \frac{v_{th}\sigma_n\sigma_p N_t(p_n n_n - n_i^2)}{\sigma_p\left[p_n + n_i e^{\frac{(E_i - E_t)}{kT}}\right] + \sigma_n\left[n_n + n_i e^{\frac{(E_t - E_i)}{kT}}\right]} \quad \text{.....(3-18)}$$

Where,

v_{th} = Thermal velocity of carriers

N_t = Concentration of the recombination center in the semiconductor

σ_n = The capture cross section of electrons

σ_p = The capture cross section of holes

The quantity σ_n describes the effectiveness of the center to capture an electron and is a measure of how close the electron has to come to the center to be captured. We can simplify

the general expression for the dependence of U on E, by assuming equal electron and hole capture cross sections, that is, $\sigma_n = \sigma_p = \sigma_o$. Equation 3-18 then becomes

$$U = V_{th}\sigma_o N_t \frac{(p_n n_n - n_i^2)}{p_n + n_n + 2n_i \cosh(\frac{E_t - E_i}{kT})} \quad \text{.....(3-19)}$$

Under a low-injection condition in an n-type semiconductor so that $n_n >> p_n$, the reconibination rate can be written as

$$U \approx V_{th}\sigma_o N_t \frac{p_n - p_{no}}{1 + \left(\frac{2n_i}{n_{no}}\right)\cosh(\frac{E_t - E_i}{kT})} = \frac{p_n - p_{no}}{\tau_p} \quad \text{.....(3-20)}$$

The recombination rate for indirect recombination is given by the same expression as Eq. 3-13; however, τ_p depends on the locations of the recombination centers.

3.3.1.3 Surface Recombination

Figure 3-5 shows schematically the bonds at a semiconductor surface. Because of the abrupt discontinuity of the lattice structure at the surface, a large number of localized energy states or generation-recombination centers may be introduced at the surface region. These energy states, called surface states, may greatly enhance the recombination rate at the surface region. The kinetics of surface reombinationare similar to those considered before for bulk centers. The total number of carriers recombining at the surface per unit area and unit time can be expressed in a form analogous to Eq. 3-18**.** For a low injection condition, and for the limiting case where electron concentration at the surfaceis essentially equal to the bulk majority carrier concentration, the total number of carriers recombining at the surface per unit area and unit time can be simplified to

$$U_s \cong v_{th}\sigma_p N_{st}(p_s - p_{no}) \quad \text{.....(3-21)}$$

Where,

P_s = Hole concentrations at the surface

N_{st} = Recombination center density per unit area in the surface region

Since the product $v_{th}\,\sigma_{np}\,N_{st}$ has its dimension in centimeters per second, it is called the low-injection surface recombination velocity S_{lr}*:*

$$S_{lr} \equiv v_{th}\sigma_p N_{st} \quad \text{.....(3-22)}$$

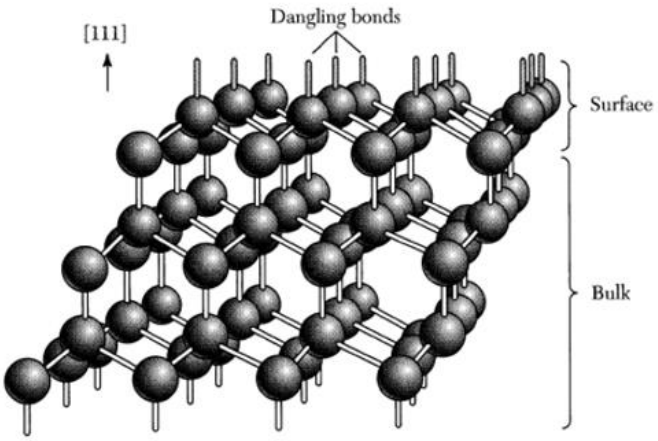

Figure 3-5 Schematic diagram of bonds at a clean semiconductor surface. The bonds are anisotropic and differ from those in the bulk

Surface recombination can have a major impact both on the short-circuit current and on the open-circuit voltage. High recombination rates at the top surface have a particularly detrimental impact on the short-circuit current since top surface also corresponds to the highest generation region of carriers in the solar cell. Lowering the high top surface recombination is typically accomplished by reducing the number of dangling silicon bonds at the top surface by using "passivating" layer on the top surface. The majority of the electronics industry relies on the use of a thermally grown silicon dioxide layer to passivate the surface due to the low defect states at the interface [18]. For commercial solar cells, dielectric layers such as silicon nitride are com m only used.

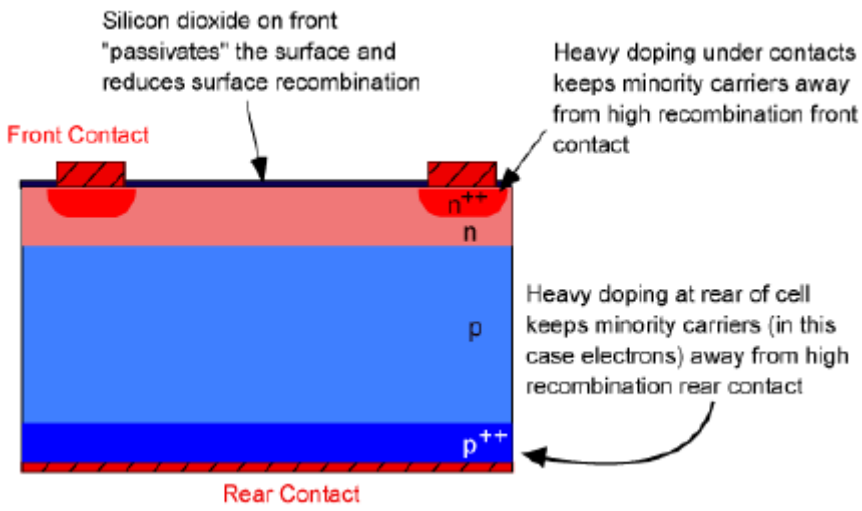

Figure 3-6 Techniques for reducing the impact of surface recombination

Since the passivating layer for silicon solar cells is usually an insulator, any region which has an ohmic metal contact cannot be passivated using silicon dioxide. Instead, under the top contacts the effect of the surface recombination can be minimized by increasing the doping. While typically such a high doping severely degrades the diffusion length, the contact regions do not participate in carrier generation and hence the impact on carrier collection is unimportant. In addition, in cases where a high recombination surface is close to the junction, the lowest recombination option is to increase the doping as high as possible.

3.3.1.3.1 Back Surface Field

A similar effect is employed at the rear surface to minimize the impact of rear surface recombination velocity on voltage and current if the rear surface is closer than a diffusion length to the junction. A "back surface field" (BSF) consists of a higher doped region at the rear surface of the solar cell. The interface between the high and low doped regions behaves like a *p*-*n* junction and an electric field forms at the interface which introduces a barrier to minority carrier flow to the rear surface. The minority carrier concentration is thus maintained at higher levels in the bulk of the dev ice and the BSF has a net effect of passivating the rear surface. [19]

3.3.1.4 Auger Recombination

The Auger recombination process occurs by the transfer of the energy and momentum released by the recombination of an electron-hole pair to a third particle that can be either an electron or a hole. The example of Auger recombination process is shown in Fig. 3-7. A second electron in the conduction band absorbs the energy released by the direct recombination. After the Auger process, the second electron becomes an energetic electron.

It loses its energy to the lattice by scattering events. Usually Auger recombination is important when the carrier concentration is very high as a result of either high doping or high injection level. Because the Auger process involves three particles, the rate of Auger recombination can be expressed as

$$R_{Aug} = Bn^2p \text{ or } Bnp^2 \quad \text{.....(3-23)}$$

The proportionality constant B has a strong temperature dependence.

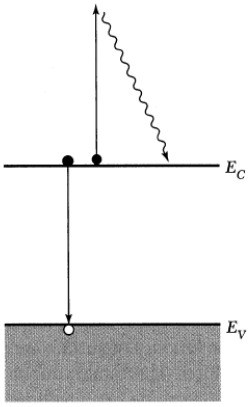

Figure 3-7 Auger recombination

3.4 Quantum Efficiency [20]

The quantum efficiency of a solar cell is defined as the ratio of the number of electrons in the external circuit produced by an incident photon of a given wavelength. Thus, one can define external and internal quantum efficiencies (denoted by EQE and IQE respectively). They differ in the treatment of photons reflected from the cell: all photons impinging on the cell surface are taken into account in the value of the EQE, but only photons that are not reflected are considered in the value of IQE.

$$EQE = \frac{Nunber\ of\ carrier\ pairs\ generated}{Number\ of\ incident\ photos} \times 100\%$$

$$IQE = \frac{Nunber\ of\ carrier\ pairs\ generated}{Number\ of\ photos\ absorbed\ by\ the\ material} \times 100\%$$

It is necessary to distinguish between internal quantum-efficiency and external quantum efficiency. External QE is the more commonly published result, and can be affected by factors ‘external’ to the diode, such as reflections, and absorption in glass layers. Internal QE considers only the collection of those photons which are incident on the junction (rather than the device). Since internal QE is not reduced by reflection/glass absorption, it always exceeds external QE, and is often close to unity over a significant spectral range.

4 Cell Optics

Flat plate solar cells in operation are illuminated from a large portion of the sky, not only because of the isotropic components of radiation, but because of the Sun's apparent motion over the day and the year if no tracking system is used. So, regarding angular distribution, these cells must accept light from the whole hemisphere. The spectral distribution also varies with time, weather conditions, etc. For calibration purposes a standard spectral distribution AM 1.5 Global is adopted as a representative condition, generally specified at $0.1 \mathrm{Wcm}^{-2}$.

4.1 Antireflection Coating

A solar cell should absorb all useful light. For non-encapsulated cells, the first optical loss is the shading by the metal grid at the illuminated face, if any. This loss is of the order of 7% for industrial cells while for laboratory cells using fine metallization it is much lower. Though several techniques have been proposed to decrease the effective shading, such as shaped fingers, prismatic covers, or cavities [21], their efficacy depends upon the direction of light and so they are not suited to isotropic illumination.

The next loss comes from the reflectance at the Si interface, more than 30% for bare Si in air due to its high refraction index. A layer of non-absorbing material with a lower refractive index (n_{ARC}) on top of the Si substrate decreases reflectance: this is a step towards the zero-reflection case of a smoothly varying refractive index [22]. If the layer is thick in terms of the coherence length of the illumination, around 1 μm for sunlight, there are no interference effects inside it. The encapsulation (glass plus lamination) belongs to this category.

The term antireflection coating (ARC) is used to refer to an optically thin dielectric layer designed to suppress reflection by interference effects. Reflection is a minimum when the layer thickness is (an odd multiple n_{ARC} of) $\lambda_0/4$, with λ_0 the free space wavelength, since in this case reflected components interfere destructively. At other wavelengths reflection increases, but is always below the value with no ARC or, at most, equal [23]. The ARC is usually designed to present the minimum at around 600 nm, where the flux of photons is a maximum in the solar spectrum. For reflection to become zero at the minimum, the coating index should be the geometric average of those of air and silicon, i.e. 2.4 at 600 nm for non-encapsulated cells. Today, the industry uses SiN_x deposited by PECVD or by sputtering for this purpose.

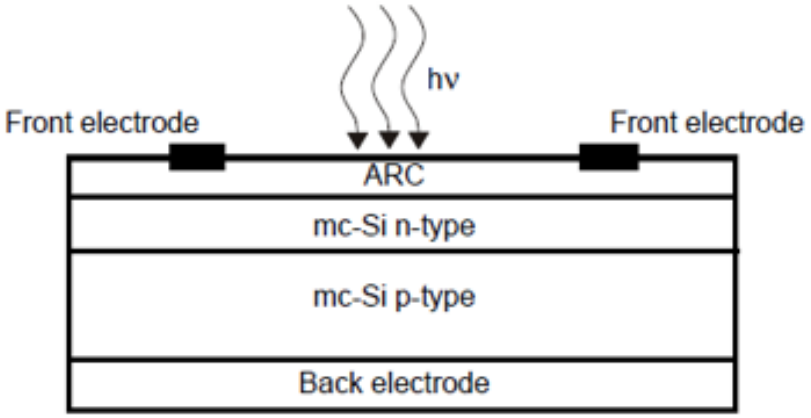

Figure 4-1 Scheme of photovoltaic solar cell with anti-reflection coating

The reflectance is defined as the fraction of incident light energy that is reflected, which is expressed by [24], [25],

$$R=\left[\frac{n-1}{n+1}\right]^2 \quad \text{.....(4-1)}$$

The thickness of the anti-reflection coating is chosen so that the wavelength in the dielectric material is one quarter the wavelength of the incoming wave. For a quarter wavelength anti-reflection coating of a transparent material with a refractive index *n* and light incident on the coating with a free-space wavelength λ_0, the thickness *d* which causes minimum reflection is calculated by:

$$d=\frac{\lambda_o}{4n} \quad \text{.....(4-2)}$$

Most solar cells rely on a thin layer of a dielectric (an antireflection coating) to reduce the reflection of light from the front surface of the cell.

The reflection coefficient from bare silicon for light incident from air is given by

$$R=\frac{(n-1)^2+k^2}{(n+1)^2+k^2} \quad \text{.....(4-3)}$$

Where n and k are the refractive index and the extinction coefficient of the semiconductor, both in general functions of the wavelength l of light in vacuum.

The extinction coefficient is related to the absorption coefficient α by

$$k = \frac{\alpha\lambda}{4\pi n}$$

For single-layer antireflection coating of refractive index n_{ar} between a top medium of refractive index n_o (for example, glass or air) and a semiconductor refractive index r_{sc}, the reflection coefficient becomes, neglecting light absorption in the semiconductor,

$$R = \frac{r_o^2 + r_{sc}^2 + 2r_o r_{sc}\cos 2\beta}{1 + r_o^2 + 2r_o r_{sc}\cos 2\beta} \quad \text{.....(4-4)}$$

Where

$$r_o = \frac{n_{ar} - n_o}{n_{ar} + n_o}; \quad r_{sc} = \frac{n_{sc} - n_o}{n_{sc} + n_o}; \quad \beta = \frac{2\pi}{\lambda} n_{ar} d$$

And d denotes the thickness of the coating. The transmission coefficient is, in both cases, simply

$$T = 1 - R$$

In most cases of interest, both r_{sc} and r_o are positive and R vanishes when

$$d = \frac{\lambda}{4n_{ar}}; \frac{3\lambda}{4n_{ar}}; \frac{5\lambda}{4n_{ar}}$$

And

$$n_{ar} = \sqrt{n_o n_{sc}}$$

The first value of d is often used in practice under the name of quarter- wavelength rule since l/n_{ar} is the wavelength of light in the antireflection coating. Reflection from the top surface can be reduced further by the use of a multilayer coating. [26]

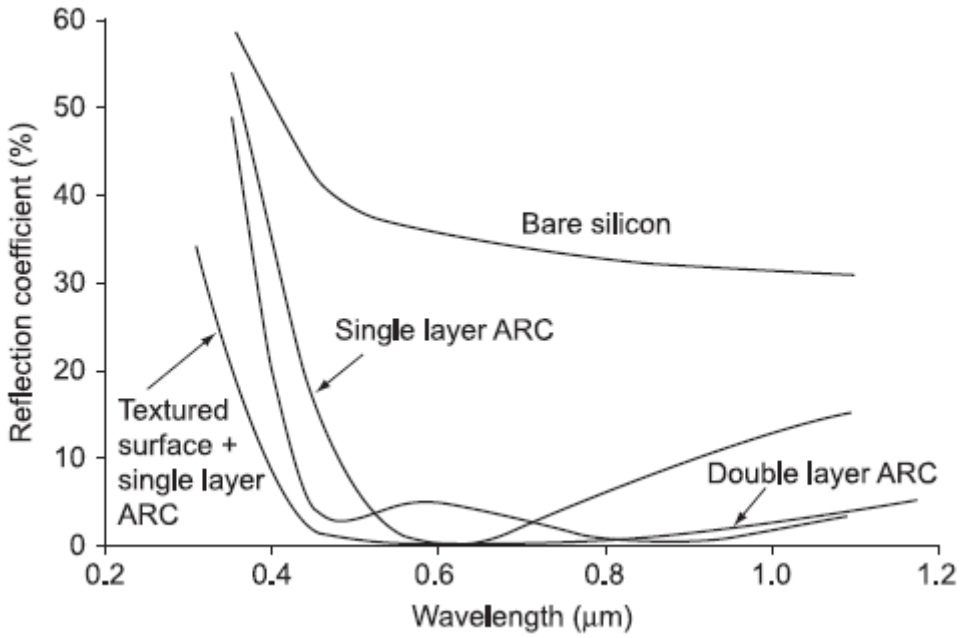

Figure 4-2 The reflection coefficient from polished bare silicon and a polished silicon surface covered with a single- and double-layer antireflection coating. The reflection coefficient for a textured surface is also shown.

The above figure compares the reflection coefficients for a smooth bare silicon surface, a smooth surface covered with antireflection coating, and a textured surface with antireflection coating.

4.1.1 ARC Deposition

Traditionally, titanium dioxide (TiO_2) was used for creating the antireflection coating due to its near optimum refractive index for encapsulated cells. A popular technique was atmospheric pressure chemical vapor deposition (APCVD) from titanium organometallic compounds and water [27]. This process is easily automated in a conveyor-belt reactor. Other possibilities included to spin-on or screen-print appropriate pastes.

But nowadays, hydrogenated silicon nitride films is the preferred option, as it combines its antireflection properties with others of bulk and surface passivation. Films can be deposited by several techniques, but the most commonly used process is chemical vapor deposition (CVD), involving the reaction of silane gas and amonnia. Plasma-enhanced chemical vapor deposition (PECVD) is preferred to other CVD technologies (atmospheric-pressure CVD or low-pressure CVD) because it is a low-temperature process (T <500 ◦C), and that means reducing complexity and preventing lifetime degradation.

PECVD techniques induce hydrogenation, whose benefits for silicon are well known [28], [29]. Amorphous silicon nitride films are produced by PECVD with up to 40 atom % of hydrogen (i.e. although these films are usually referred to as SiN_x they are really a-SiN_x:H). A subsequent thermal step is needed to activate hydrogenation, and in an industrial process metal firing step fulfills this objective [30].

In "direct" PECVD, schematized in Figure 4-3a, the processing gasses are excited by means of an electromagnetic field, and the wafers are located within the plasma. Bulk is effectively passivated, but surface damage is produced due to direct exposition of wafers to plasma, precluding the achievement of good surface passivation. Furthermore, surface passivation degrades with exposition to UV light.

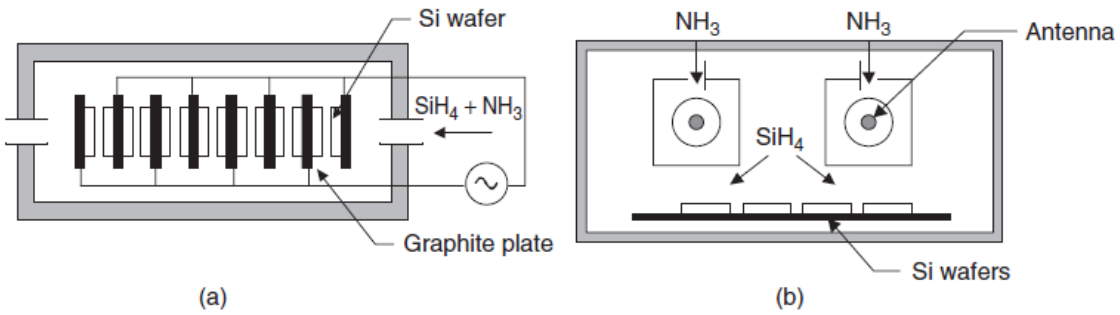

Figure 4-3 Industrial PECVD reactors. (a) Direct-plasma reactor; (b) remote-plasma system

There is a high-frequency direct PECVD (13.56 MHz) and a low-frequency one (in the range 10–500 kHz), the former being better in terms of surface passivation and UV stability. On the other hand, it is more difficult to obtain uniform layers.

A different approach is the "remote" PECVD, where wafers are located outside the region where the plasma is formed. Surface damage is avoided in this way, so that better surface passivation is achieved. On the other hand, bulk passivation is reduced. Figure 4-3b shows a sketch of an industrial remote PECVD. It implements a continuous feed of wafers, an advantage that should be compared with the batch-type direct PECVD.

Another technology able to achieve similar surface and bulk passivation properties as those of PECVD is sputtering [31], with the advantage of avoiding the use of the pyrophoric silane gas. For this process, wafers are moved horizontally through the in-line system, where silicon targets are alternately sputtered in argon and nitrogen to deposit the silicon

nitride film onto the silicon wafer. Nitrogen and ammonia may be added to vary the refractive index and the hydrogen content of the film.

4.2 Texturing

Alkaline solutions etch a Si crystal anisotropically, exposing {111} planes on which the etching rate is lowest. On [1 0 0]–oriented wafers, randomly distributed, square pyramids are formed who's size is adjusted to a few micrometers by controlling etching time and temperature. In a textured face, a ray can be reflected towards a neighboring pyramid (Figure 4-4a) and hence absorption is enhanced. Though calculation of reflection requires ray tracing, a rough estimate for near-normal incidence can be derived by assuming each ray strikes the Si surface twice so that reflection is the square of the un textured case. As multi crystalline substrates lack a single crystal orientation, alkaline etches are not efficient, and several alternatives are proposed to achieve similar effects of reflection reduction. Texturing is incorporated in both industrial and laboratory Si solar cells, and, in combination with AR coating, reduces reflection losses to a few percent. In the latter case, in order to better control the pyramid geometry and to allow delineation of fine features on the surface, photolithographic techniques are used to define inverted or upright pyramids at the desired positions. It has to be noted that in this case the reflectivity is similar to that of a random texture [32].

Light entering the substrate at a textured surface is tilted with respect to the cell normal. This means that photo generation takes place closer to the collection junction, which is very beneficial for low-diffusion-length cells by enhancing the collection efficiency for medium to long wavelengths (Figure 4-4b). The effect is equivalent to an increase of the absorption coefficient. As a drawback, textured surfaces present higher SRVs.

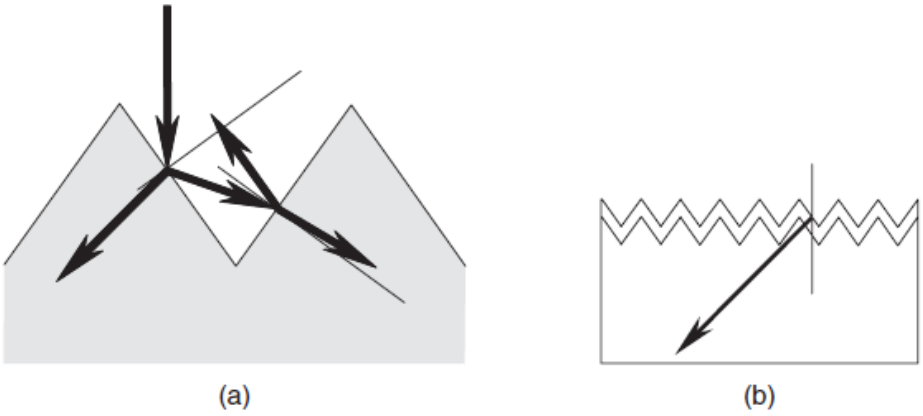

Figure 4-4 Effects of surface texturing: (a) decreased reflection; (b) increased photogeneration in

4.2.1 Texturing process

Surface texturing can be accomplished in a number of ways. A single crystalline substrate can be textured by etching along the faces of the crystal planes. The crystalline structure of silicon results in a surface made up of pyramids if the surface is appropriately aligned with respect to the internal atoms. One such pyramid is illustrated in the drawing below. An electron microscope photograph of a textured silicon surface is shown in the photograph below. This type of texturing is called "random pyramid" texture, and is commonly used in industry for single crystalline wafers.

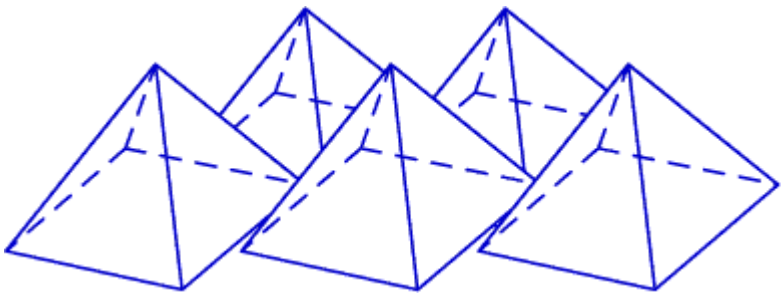

Figure 4-5 A square based pyramid which forms the surface of an appropriately textured crystalline silicon solar cell

Another type of surface texturing used is known as "inverted pyramid" texturing [33], [34]. Using this texturing scheme, the pyramids are etched down into the silicon surface rather than etched pointing upwards from the surface. A photograph of such a textured surface is shown below.

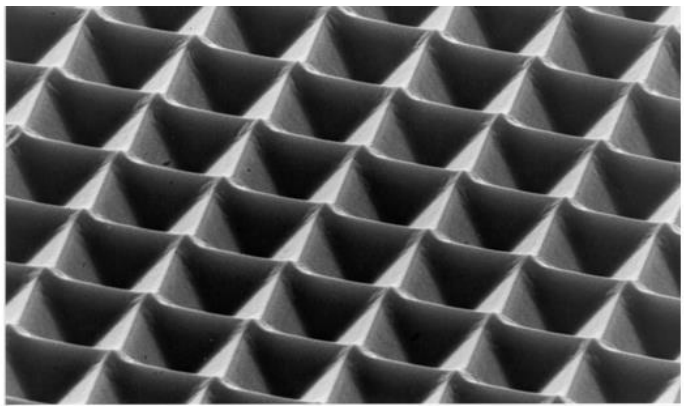

Figure 4-6 Scanning electron microscope photograph of a textured silicon surface

For multi crystalline wafers, only a small fraction of the surface will have the required orientation of <100> and consequently these techniques are less effective on multi crystalline wafers. However, multi crystalline wafers can be textured using a photolithographic technique [35] as well as mechanically sculpting the front surface using dicing saws [36] or lasers [37] to cut the surface into an appropriate shape. A micrograph of a photolithographic texturing scheme is shown below.

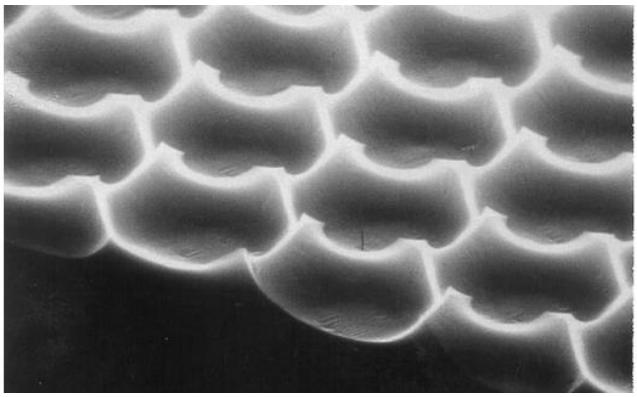

Figure 4-7 Scanning electron microscope photograph of a textured multicrystalline silicon surface

5 Results and Discussions

Design of device parameters is a crucial step for a solar cell preparation. To find the values of device parameters of a crystalline silicon solar which will predict the optimum value of solar cell efficiency and performance, a c-silicon solar cell has been simulated using PC1D simulation software and varying the device parameter values the effects were studied and optimum values were selected.

5.1 Characteristics of a normal solar cell

Assumptions:

Device Area	: 100 cm^2
Exterior Front Reflectance	: 35 %
Cell Thickness	: 80 µm
Di-electric Constant	: 11.9
Band Gap	: 1.124 ev
Intrinsic Conc. at 300K	: 1×10^{10} cm^{-3}
P-type Doping	: 1×10^{16} cm^{-3}
N-type Doping	: 1×10^{17} cm^{-3}

5.1.1 I-V Characteristics

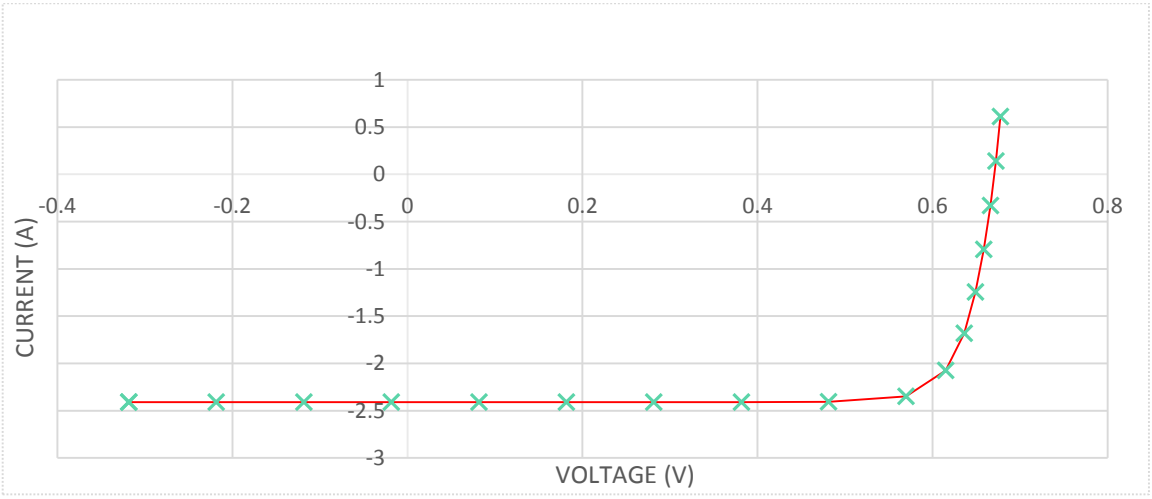

Figure 5-1 I-V characteristics of a basic solar cell

From the above curve, I_{sc} was found as -2.408 A and V_{oc} was found as 0.6705 V for a bare crystalline silicon solar cell.

5.1.2 P-V Characteristics

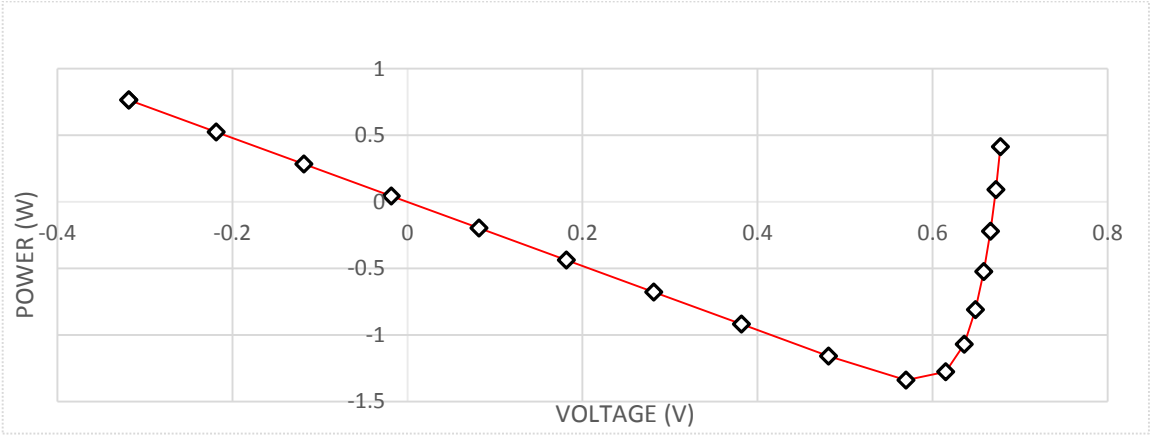

Figure 5-2 P-V characteristics of a basic solar cell

From the above curve, P_{max} was found as 1.346 W for a bare crystalline solar cell.

5.1.3 EQE-Wave Length Characteristice

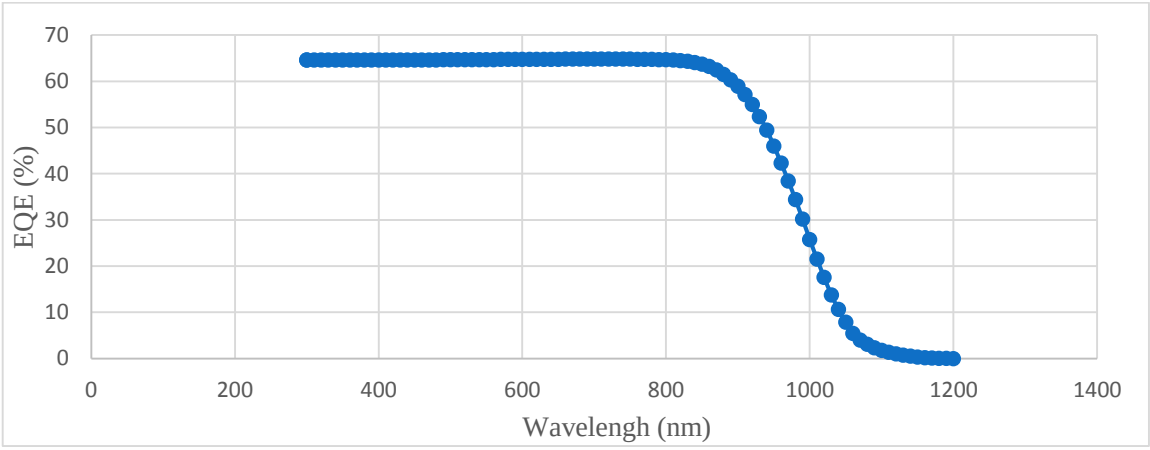

Figure 5-3 EQE-Wave Length characteristics of a basic solar cell

From the above curve, EQE was found 64% for a bare crystalline solar cell.

5.1.4 Outcome of the study in tabular form

Table 5-1 Result for bare silicon solar cell

I_{sc} (A)	V_{oc} (V)	P_{max} (W)	EQE
-2.408	0.6705	1.346	64%

5.2 Effect of the surface area on the efficiency

Here the effect of surface area were identified varying the surface area and keeping all the other parameters as above.

Assumptions :

(a) Surface of 100 cm^2
(b) Surface of 150 cm^2
(c) Surface of 200 cm^2

5.2.1 I-V Characteristics

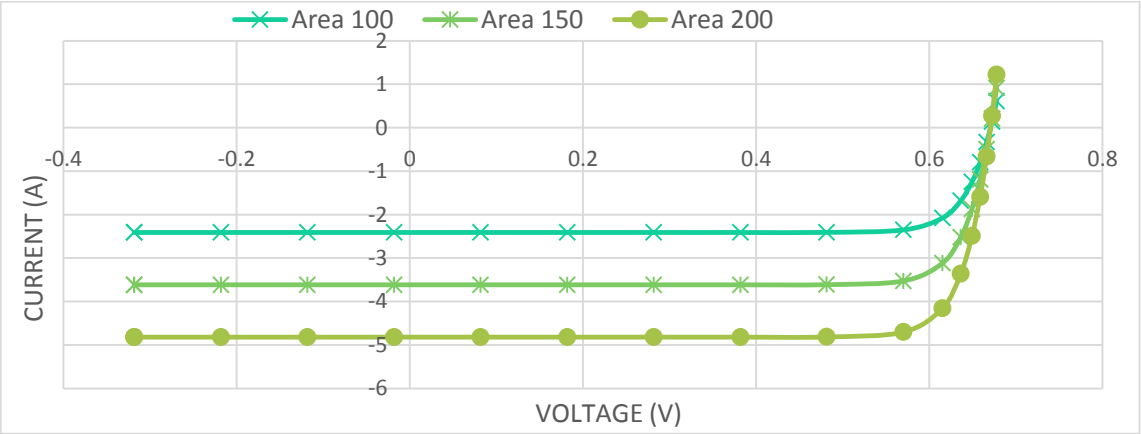

Figure 5-4 Effect of the surface area on the efficiency, I-V characteristics

From the above curves, I_{sc} values were found to be -2.408 A, -3.618 A and -4.816 A respectively for (a), (b) and (c) options and V_{oc} were same for the three curve which was 0.6705 V.

5.2.2 P-V Characteristics

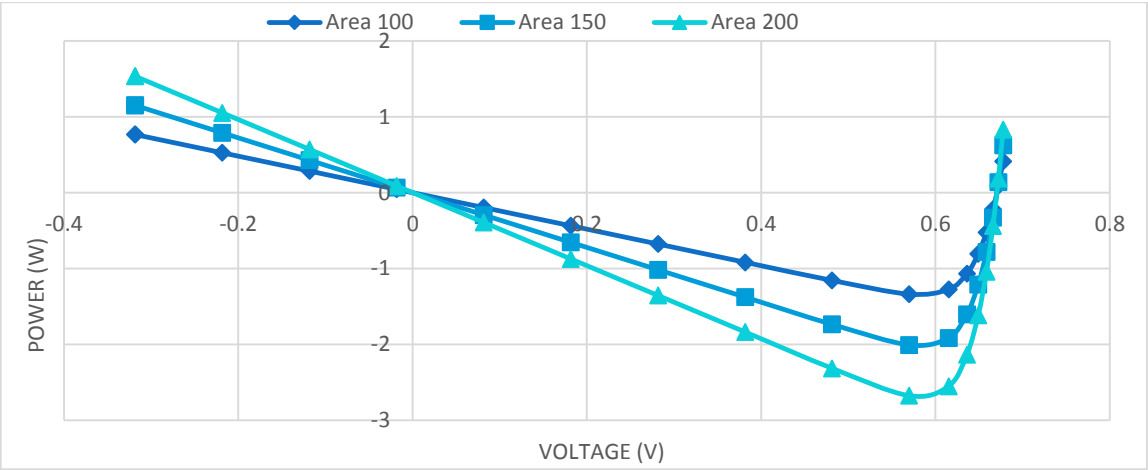

Figure 5-5 Effect of the surface area on the efficiency, P-V characteristics

From the above curves, P_{max} values were found to be 1.346 W, 2.019 W and 2.692W respectively for (a), (b) and (c) options.

5.2.3 EQE-Wave Length Characteristics

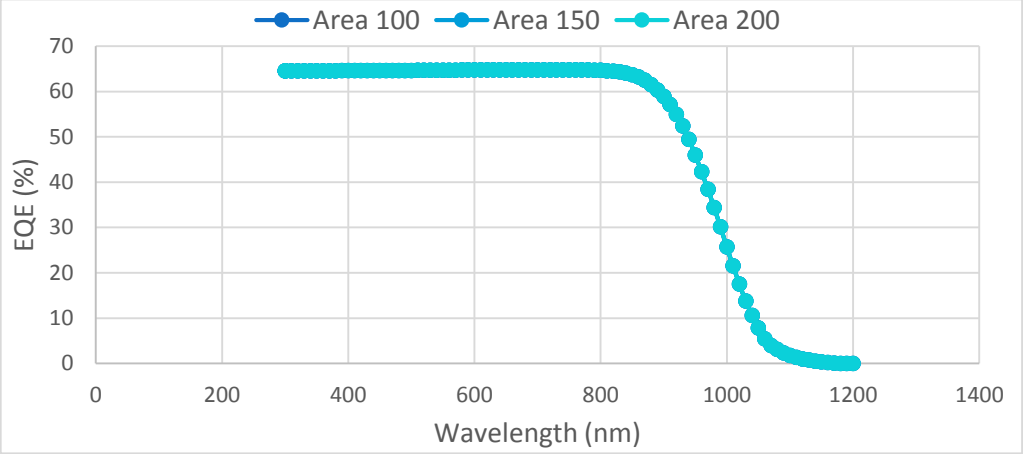

Figure 5-6 Effect of the surface area on the efficiency, EQE-Wave Length characteristics

From the above curve, EQE was found almost same for (a), (b) and (c) options.

5.2.4 Outcome of the study in tabular form

Table 5-2 Result for varying surface area

Surface Area	I_{sc} (A)	V_{oc} (V)	P_{max} (W)
100 cm^2	-2.408	0.6705	1.346
150 cm^2	-3.612	0.6705	2.019
200 cm^2	-4.816	0.6705	2.692

5.3 Effect of the thickness of n and p region on the efficiency

For this case study, the device parameter were kept same as the ordinary basic silicon solar cell and the thickness of n and p region of the cell were changed.

Assumptions :

(a) Thickness of N and P : 5 µm & 75 µm
(b) Thickness of N and P : 20 µm & 60 µm
(c) Thickness of N and P : 30 µm & 50 µm
(d) Thickness of N and P : 40 µm & 40 µm

5.3.1 I-V Characteristics

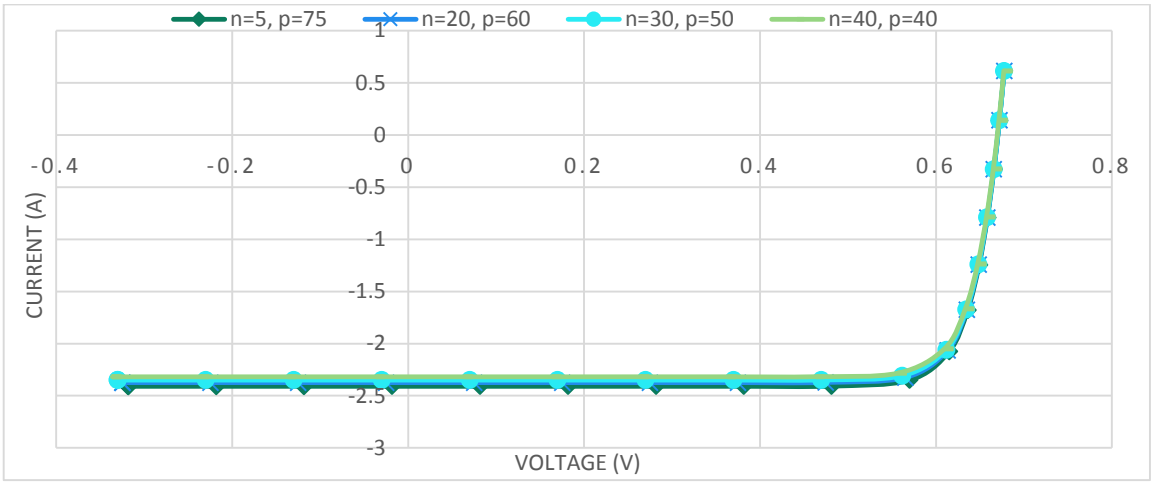

Figure 5-7 Effect of the thickness of n and p region on the efficiency, I-V characteristics

From the above curves, short circuit current, I_{sc} values were found to be -2.408 A, -2.375 A, 2.349 A and -2.319 A respectively for (a), (b), (c) and (d) options and V_{oc} values were almost same for the above four curves. It indicated that the declination of I_{sc} occurs with the raise of the thickness of n region.

5.3.2 P-V Characteristics

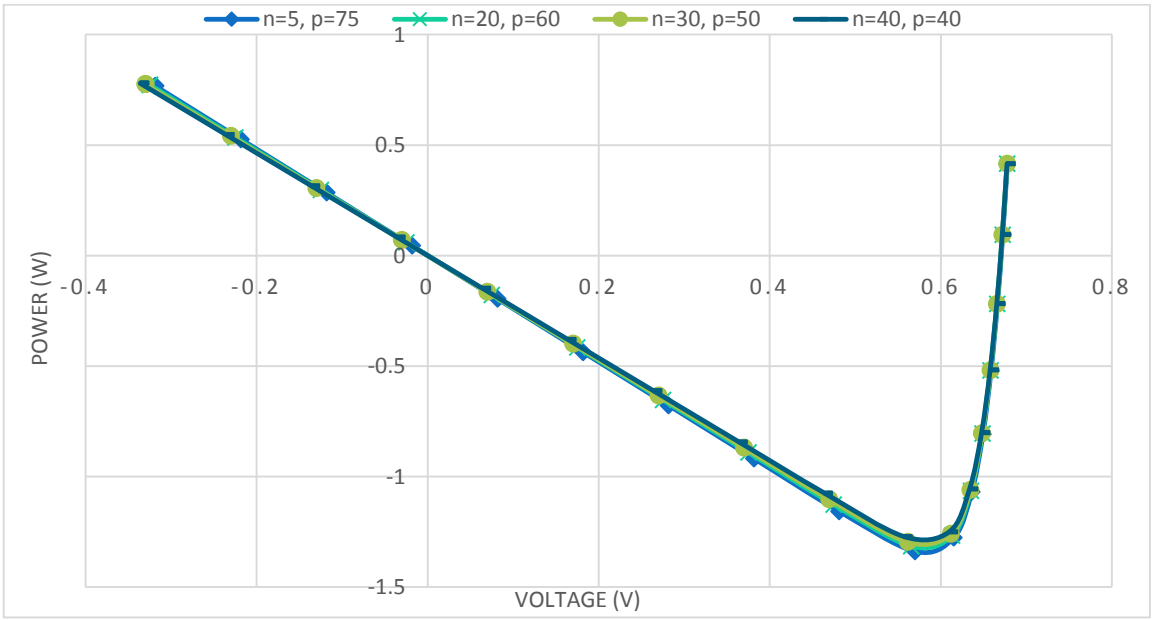

Figure 5-8 Effect of the thickness of n and p region on the efficiency, P-V characteristics

From the above curves, P_{max} were found as 1.346 W, 1.325 W, 1.309 W and 1.289 W respectively for (a), (b), (c) and (d) options. It indicated that the declination of P_{max} occurs with the raise of the thickness of n region.

5.3.3 EQE-Wave Length Characteristics

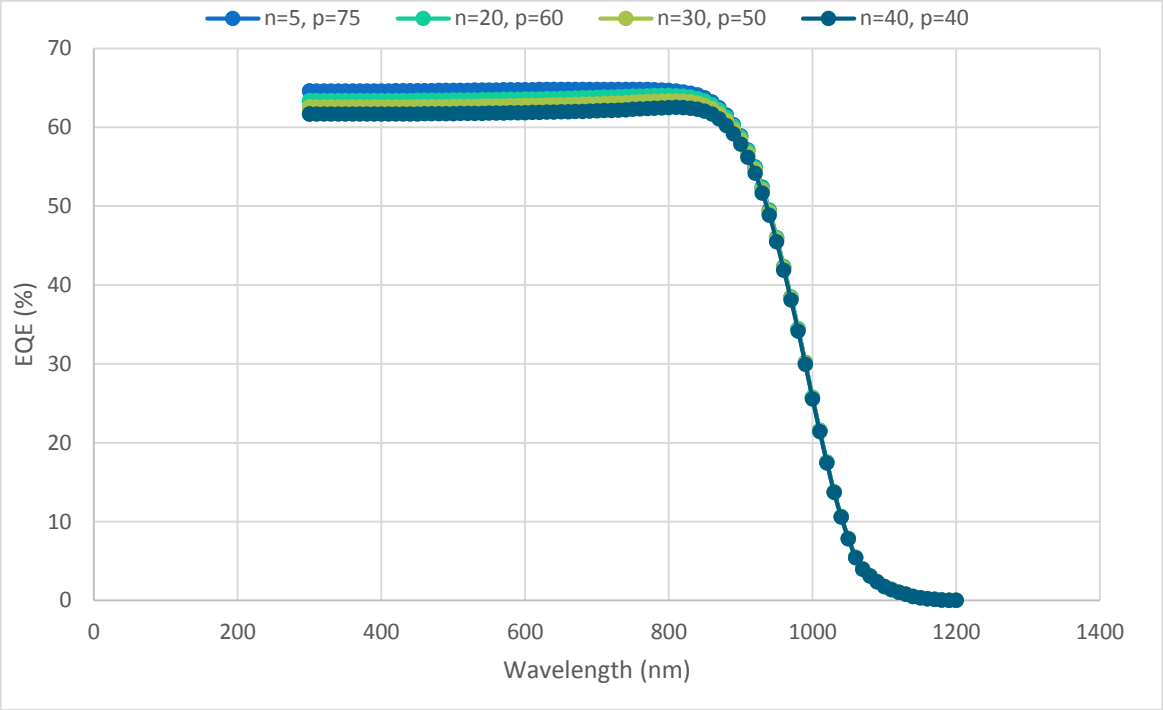

Figure 5-9 Effect of the thickness of n and p region on the efficiency, EQE-Wave Length characteristics

From the above curve, it was found that the EQE was decreasing with the increase of thickness of the top layer of the solar cell, n region.

5.3.4 Outcome of the study in tabular form

Table 5-3 Result for varying thickness of n and p region

Device Thickness (µm)	n Region Thickness (µm)	p Region Thickness (µm)	I_{sc} (A)	V_{oc} (V)	P_{max} (W)
80	5	75	-2.408	0.6705	1.346
80	20	60	-2.375	0.6703	1.325
80	30	50	-2.349	0.6701	1.309
80	40	40	-2.319	0.6698	1.289

5.4 Effect of the doping of p++ on the efficiency

For this case study, the effect of the doping of BSF layer, p++ layer was studied keeping all the device parameters same as above.

Assumptions :

(a) Doping p++ : $1 \times 10^{18} cm^{-3}$
(b) Doping p++ : $1 \times 10^{19} cm^{-3}$
(c) Doping p++ : $1 \times 10^{20} cm^{-3}$

5.4.1 I-V Characteristic

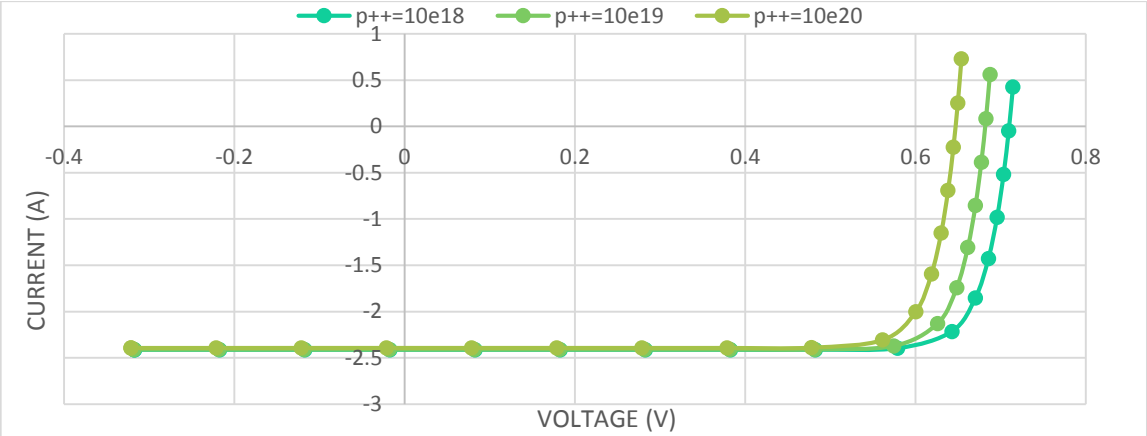

Figure 5-10 Effect of the doping of p++ on the efficiency, I-V characteristics

From the above curves, I_{sc} values were found as -2.413 A, -2.410 A and -2.393 A respectively for (a), (b) and (c) options. V_{oc} values were found as 0.7101 V, 0.6819 V and 0.6469 V respectively for (a), (b) and (c) options. The maximum values of I_{sc} and v_{oc} were found for acceptor doping density of p++ at $1 \times 10^{18} cm^{-3}$.

5.4.2 P-V Characteristics

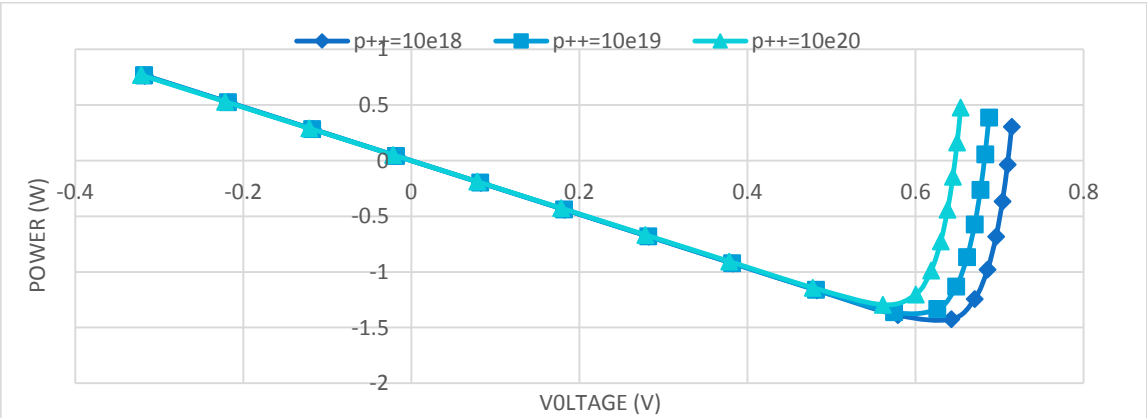

Figure 5-11 Effect of the doping of p++ on the efficiency, P-V characteristics

From the above curves, P_{max} values were found as 1.436 W, 1.378 W and 1.297 W respectively for (a), (b) and (c) values. It indicated that the declination of P_{max} occured with the raise of the p++ doping.

5.4.3 EQE-Wave Length Characteristics

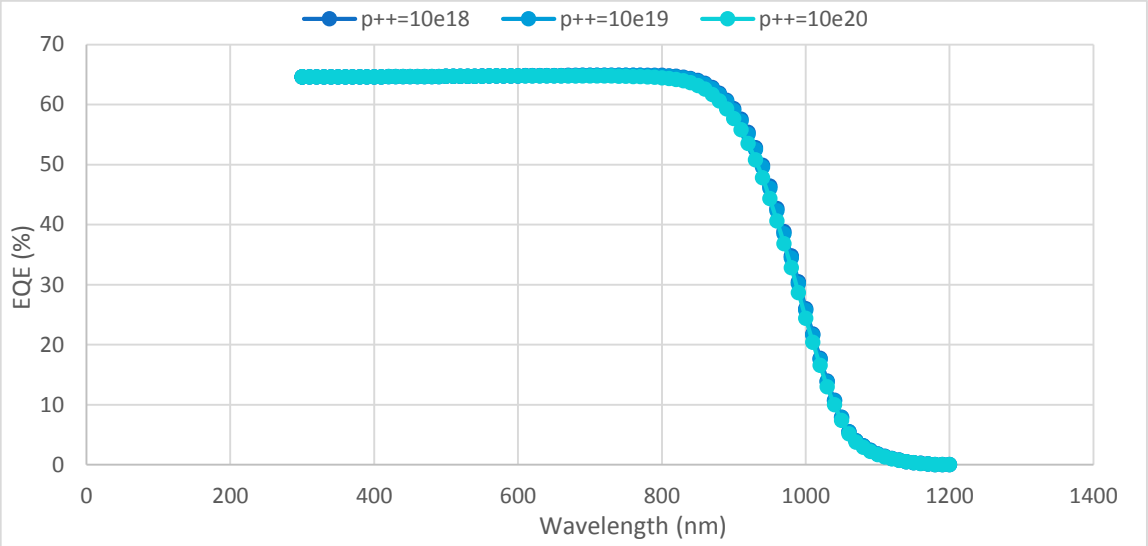

Figure 5-12 Effect of the doping of p++ on the efficiency, EQE-Wave Length characteristics

From the above curves, it was found that there was no significant change in the EQE except little increase EQE at higher wavelength which has no major importance.

5.4.4 Outcome of the study in tabular form

Table 5-4 Result for varying p++ doping

Doping p++	I_{sc} (A)	V_{oc} (V)	P_{max} (W)
1×10^{18} cm^{-3}	-2.413	0.7101	1.436
$1\times 10^{19}cm^{-3}$	-2.410	0.6819	1.378
1×10^{20} cm^{-3}	-2.393	0.6469	1.297

5.5 Effect of the thickness of p++ layer on the efficiency

Assumption :

(a) Thickness P++ : 15 µm

(b) Thickness P++ : 10 µm

(c) Thickness P++ : 5 µm

(d) Thickness P++ : 1 µm

5.5.1 I-V Characteristics

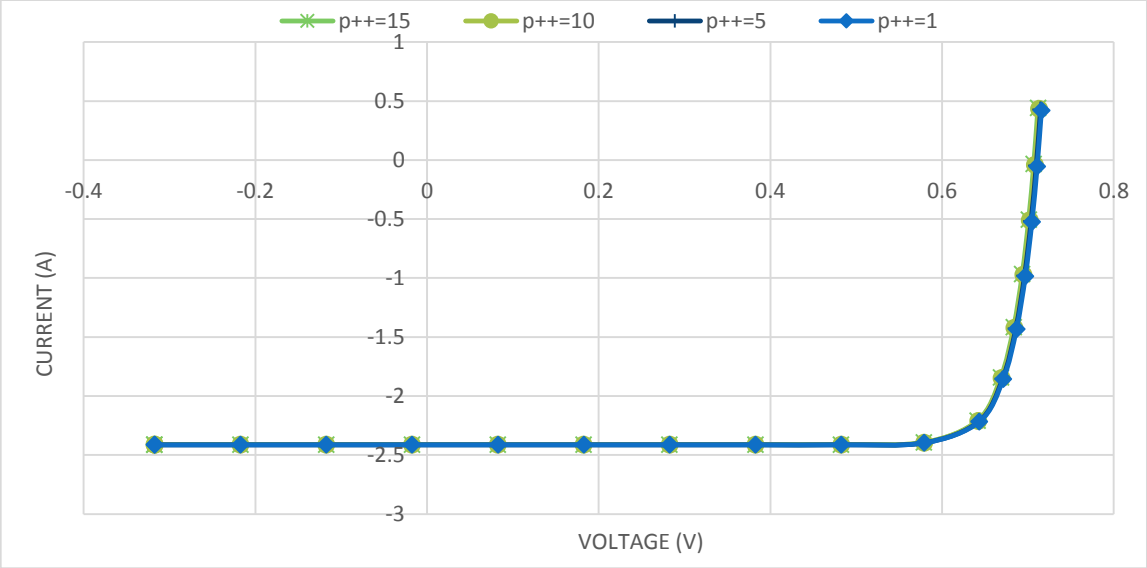

Figure 5-13 Effect of the thickness of p++ layer on the efficiency, I-V characteristics

From the above curves, I_{sc} values were found as -2.412 A, -2.413 A, -2.413 A and -2.413 A respectively for (a), (b), (c) and (d) options. V_{oc} values were found as 0.7072 V, 0.7085 V, 0.7101 V and 0.7114 V respectively for (a), (b), (c) and (d) options. It indicated that there was no significant change of I_{sc} value but there was a little increase of V_{oc} occured with the decrease of the thickness of p++ region.

5.5.2 P-V Characteristics

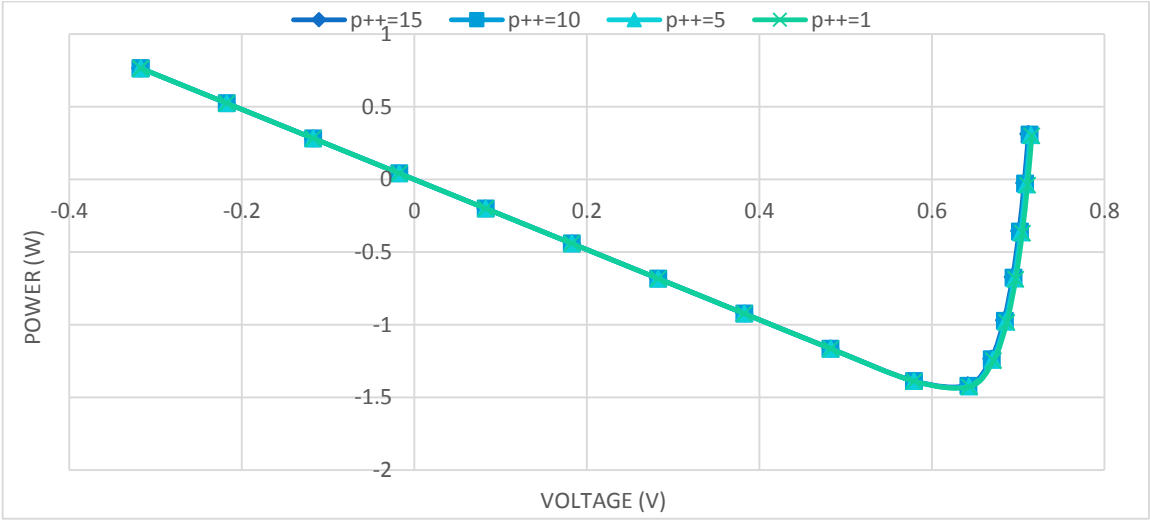

Figure 5-14 Effect of the thickness of p++ layer on the efficiency-V characteristics

From the above curves, P_{max} values were found as 1.430 W, 1.433 W, 1.436 W and 1.438 W respectively for (a), (b), (c) and (d) options. It indicated that there was a little raise of P_{max} occured with the declination of the thickness of p++ region.

5.5.3 EQE-Wave Length Characteristics

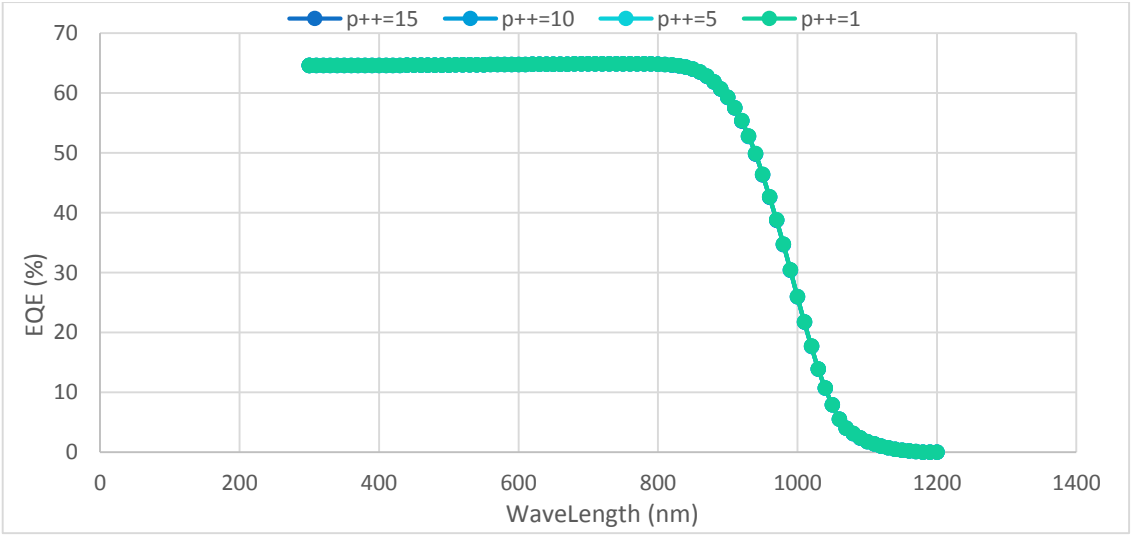

Figure 5-15 Effect of the thickness of p++ on the efficiency, EQE-Wave Length characteristics

From the above curve, it was found that there was no significant change in the EQE with the variation of the thickness of p++ region.

5.5.4 Outcome of the study in tabular form

Table 5-5 Result for varying thickness of p++ layer

Thickness of p++	I_{sc} (A)	V_{oc} (V)	P_{max} (W)
1 μm	-2.413	0.7114	1.438
5 μm	-2.413	0.7101	1.436
10 μm	-2.413	0.7085	1.433
15 μm	-2.412	0.7072	1.430

5.6 Effect of the anti-reflection coating on the efficiency

A significant portion of optical energy is reflected which reduces the external quantum efficiency. An adequate layer of antireflection coating can be used to reduce the reflection. Here different antireflection coating were investigated to find the apt one for a crystalline silicon solar cell.

Assumptions :

(a) MnO_2
(b) ZnO_2
(c) Si_3N_4
(d) TiO_2

5.6.1 I-V Characteristics

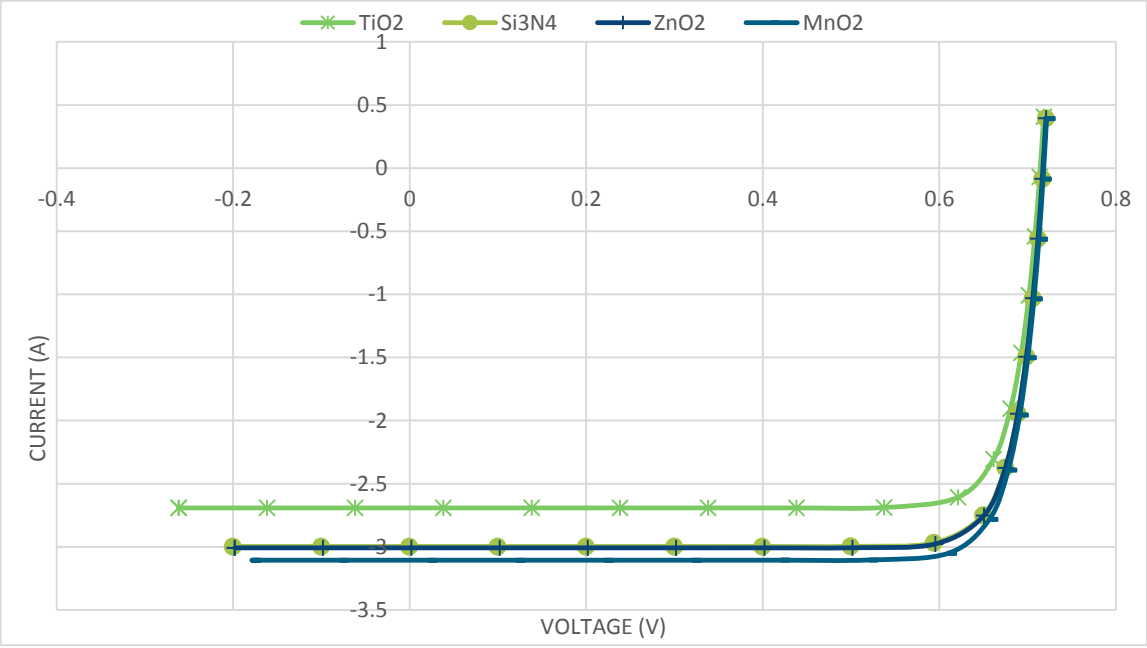

Figure 5-16 Effect of the anti-reflection coating on the efficiency, I-V characteristics

From the above curves, I_{sc} values were found as -3.106 A, -3.009 A, 2.997 A and -2.691 A respectively for (a), (b), (c) and (d) options and V_{oc} value was changed a little for different options types of anti-reflection layers. The best value of I_{sc} was found for MnO_2.

5.6.2 P-V Characteristics

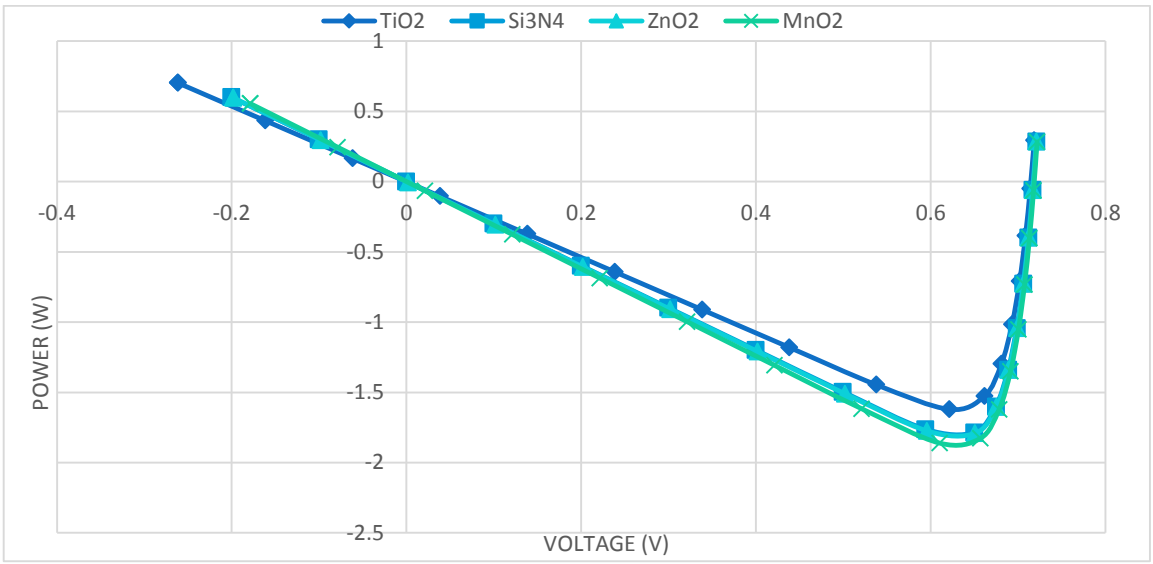

Figure 5-17 Effect of the antireflection coating on the efficiency, P-V characteristics

From the above curves, P_{max} values were found as 1.882 W, 1.809 W, 1.802 W and 1.623 W respectively for (a), (b), (c) and (d) options. The best P_{max} value was found for MnO_2.

5.6.3 EQE-Wave Length Characteristics

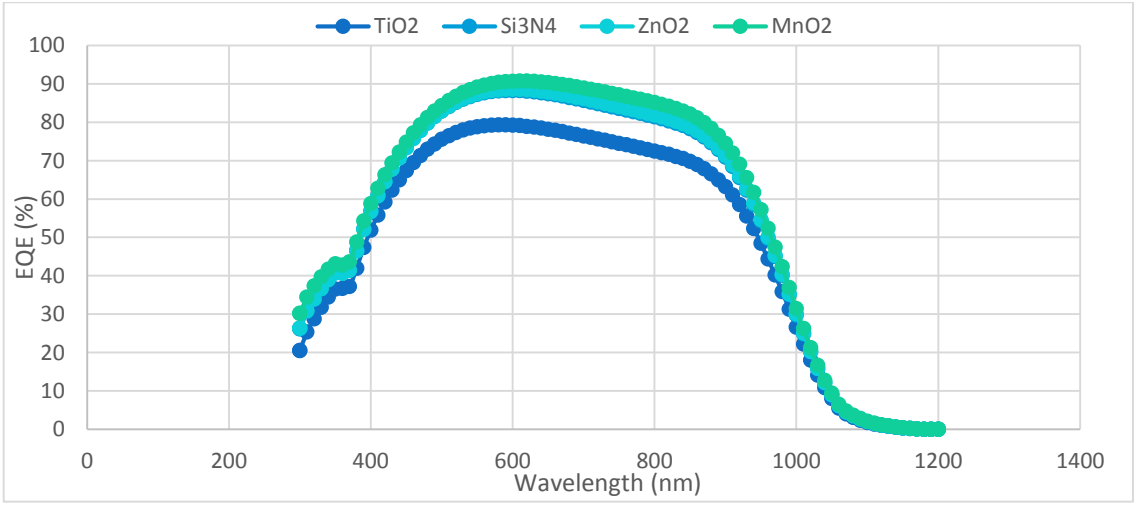

Figure 5-18 Effect of the anti-reflection coating on the efficiency, EQE-Wave Length characteristics

From the above curves, it was found that there was very significant change in the EQE for different ARC compared to bare silicon solar cell. EQE value increased for all ARC and the best EQE value was found almost 94% for MnO_2.

5.6.4 Outcome of the study in tabular form

Table 5-6 Result for different antireflection coating

ARC	Reflective Index **(n)**	Thickness **(λo)**	I_{SC} (A)	V_{OC} (V)	P_{max} (W)
MnO_2	1.7355	86.4 nm	-3.106	0.7183	1.882
ZnO_2	2	75 nm	-3.009	0.7174	1.809
Si_3N_4	2.02	74 nm	-2.997	0.7173	1.802
TiO_2	2.4	62.5 nm	-2.691	0.7144	1.623

5.7 Effect of the texturing angle on the efficiency

Assumption :

(a) Textured angle : 50 degree
(b) Textured angle : 60 degree
(c) Textured angle : 61 degree
(d) Textured angle : 62 degree
(e) Textured angle : 70 degree
(f) Textured angle : 81 degree

5.7.1 I-V Characteristics

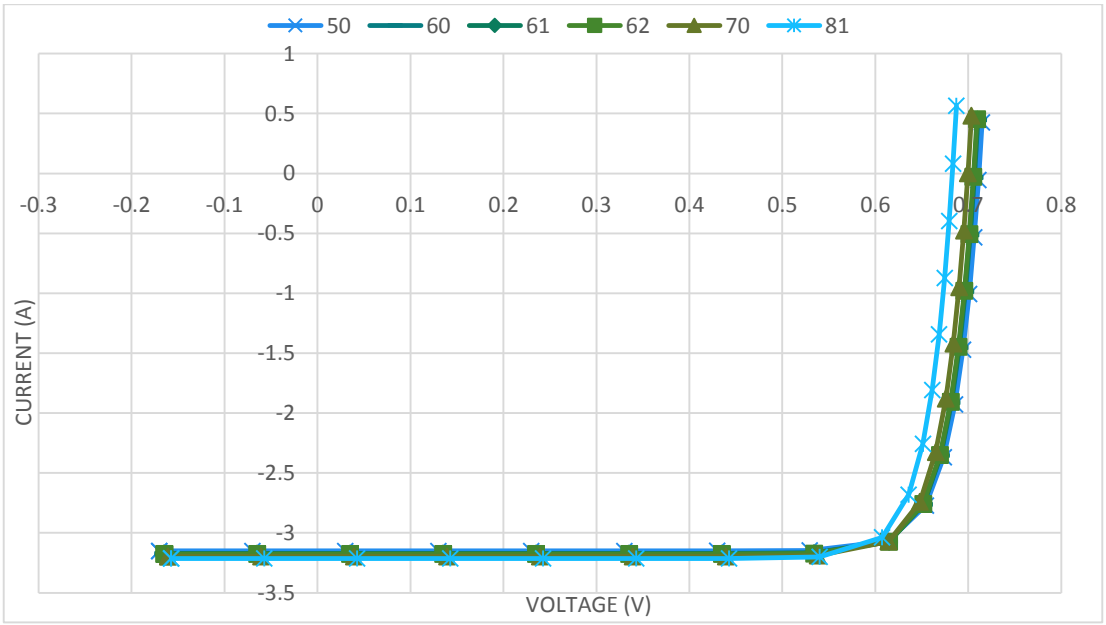

Figure 5-19 Effect of the texturing angle on the efficiency, I-V characteristics

From the above curves, I_{sc} values were found slightly increasing but V_{oc} values were found slightly decreasing with the increase of texturing angle from (a) to (f) options.

5.7.2 P-V Characteristics

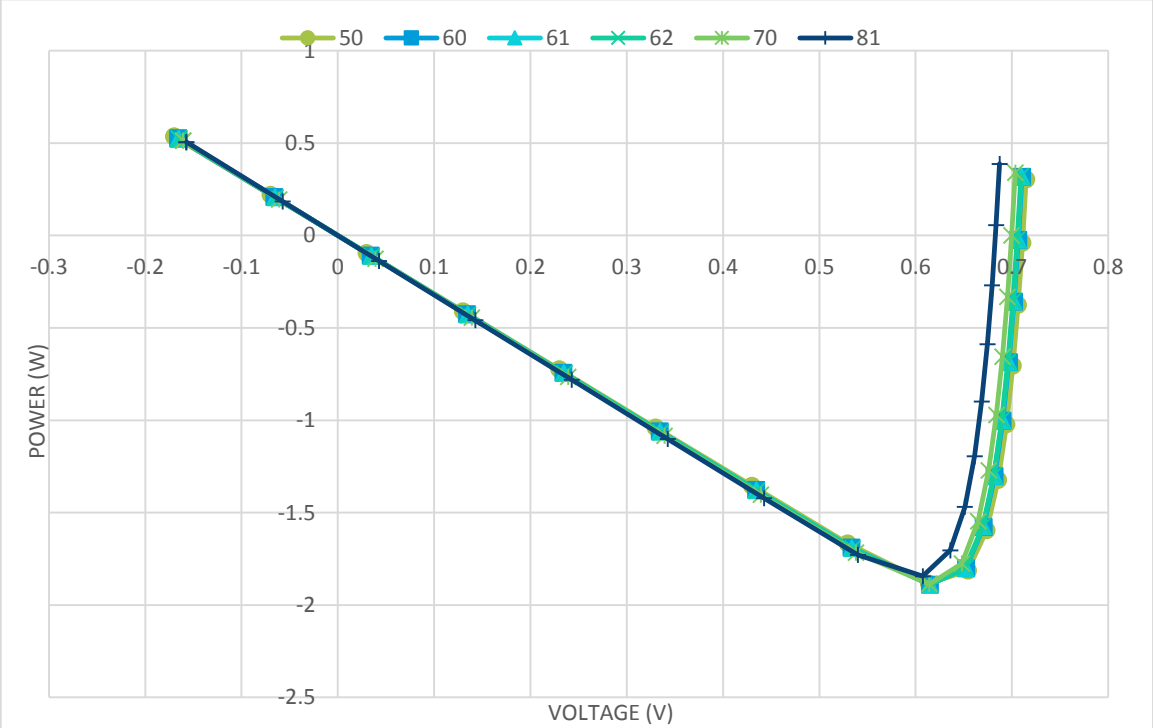

Figure 5-20 Effect of the texturing angle on the efficiency, P-V characteristics

From the above curves, P_{max} values were found increasing for (a) to (c) options and then decreasing from (d) up to (f) options.

5.7.3 EQE-Wave Length Characteristics

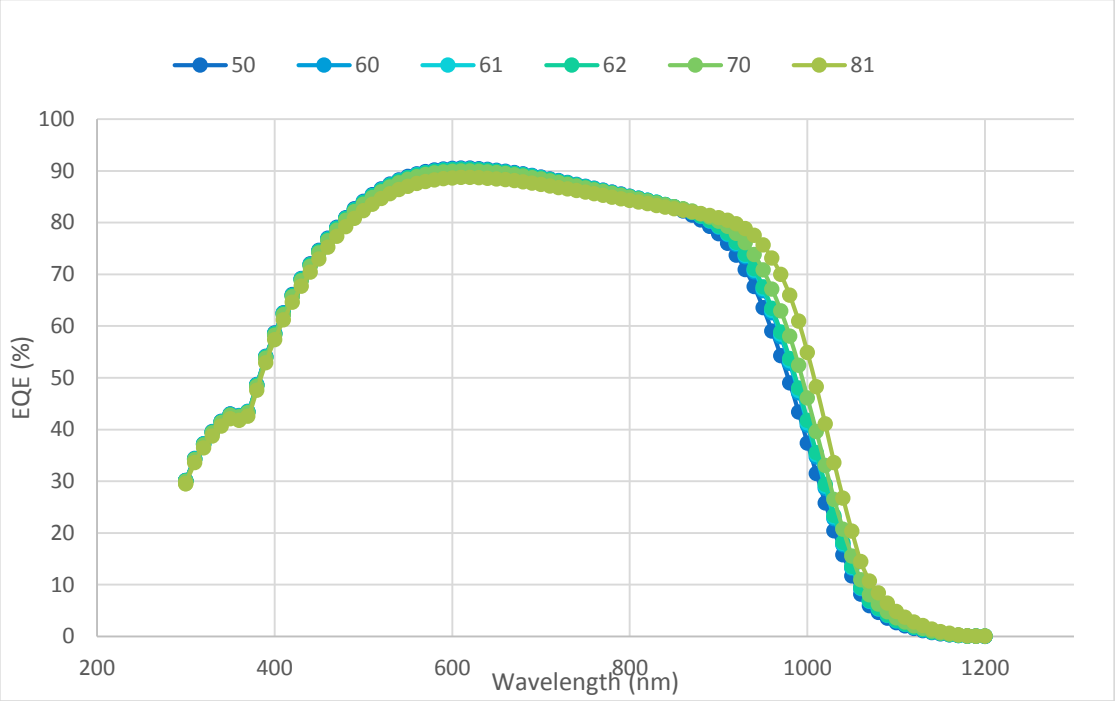

Figure 5-21 Effect of the texturing angle on the efficiency, EQE-Wave Length characteristics

From the above curves, EQE values were found increasing at higher wavelengths but slightly decreasing at lower wavelengths with the increase of texturing angle from (a) to (f) options.

5.7.4 Outcome of the study in tabular form

Table 5-7 Result for different texturing angle

Texturing Angel	I_{SC} (A)	V_{OC} (V)	P_{max} (W)
50	-3.150	0.7113	1.894
60	-3.171	0.7069	1.895
61	-3.174	0.7063	1.895
62	-3.176	0.7057	1.894
70	-3.196	0.6996	1.888
81	-3.214	0.6829	1.845

6 Conclusion

The simulation experiment has been carried out utilizing three the standard semiconductor Poisson's equation, Continuity equation and Current Density equation incorporated in the version 5.19 of PC1D simulator, developed by the University of New South Wales, Australia.

The absorption of photons increases with the increase of cell surface area Thus, the current and power of a solar cell increases. Minimum thickness of top n-layer allow the photons to create electron-hole pairs near p-n junction. Thus, more current and power is found with the decrease of top n layer thickness. Optimum result found for the solar cell thickness of 80μm.

The rate of depletion of minority carriers is reduced by limiting the surface recombination. The power output increases with the doping rates of the Back Surface Field (BSF). A highly doped BSF of p++ layer of $1 \times 10^{18} cm^{-3}$ at the bottom of the solar cell with carrier densities of $1 \times 10^{17} cm^{-3}$ of n layer, $1 \times 10^{16} cm^{-3}$ for p layer. The voltage and current of the solar cell increases slightly with decrease of BSF layer thickness.

Antireflection coating decreases reflection of incident light. For a suitable antireflection coating current as well as power increases. For an anti-reflection coating of MnO_2 performance improves. The external quantum efficiency can be 64% to around 95%. Efficiency increases from 13.46% to 18.82%

Light reflects more from plain surface than rough surface. In plain surface, around 30-35% incident light bounce back directly. For high angle texturing, the absorption of light increases at higher wavelengths. But decreases at visible wavelengths, which is undesirable for a solar energy applications. A significant amount of the can be trapped with a textured surface of texture angle of 61 degrees and the efficiency increases from 18.82% with ARC only to 18.95% with ARC and textured surface concept.

References

[1] R. S. Ohl, "Light sensitive electric device". USA Patent 240252, 1941.

[2] M. A. Green, "The path to 25% silicon solar cell efficiency: History of silicon cell evolution," *Progress in Photovoltaics,* vol. 17(3), pp. 183-189, 2009.

[3] L. Chapin, "A new silicon p-n junction photocell for converting solar radiation into electrical power," *Journal of Applied Physics,* vol. 25, pp. 676-677, 1954.

[4] J. Perlin, From space to earth, Ann Arbor, Michigan: AATEC publications, 1999.

[5] M. Wolf, "The effects of a drift field on solar cells," in *Proceedings of the 3rd IEEE Photovoltaic Specialists Conference*, Washington, 1963.

[6] W. N. Hess, "The effects of high altitude explosions," *Space Physics,* pp. 573-610, 1964.

[7] P. Mandelkorn, "Fabrication and characteristics of phosphorous-diffused silicon solar cells," *Journal of the Electrochemical Society,* vol. 109(4), pp. 313-318, 1962.

[8] A. Blakers, "20% efficiency silicon solar cells," *Applied Physics Letters,* vol. 48(3), pp. 215-217, 1986.

[9] A. Blakers, "22.8% efficient silicon solar cells," *Applied Physics Letters,* vol. 55(3), pp. 1363-1365, 1989.

[10] A. Zhao, "24% efficient silicon solar cells," in *Proceedingfs of the 1st World Conference on PV Energy Conversion*, Hawaii, USA, 1994.

[11] M. Sinton, "27.5% silicon concentrator solar cells," *IEEE Electron Device Letters,* vol. 7(10), pp. 567-569, 1986.

[12] R. M. Swanson, "Point-contact solar cells: modeling and experiment," *Solar Cells,* vol. 17(1), pp. 85-118, 1986.

[13] A. Zhao, "24.5% Efficiency silicon PERT cells on MCZ substrates and 24.7% efficiency PERL cells on FZ substrates," *Progress in Photovoltacis: Research and Applications,* vol. 7(6), pp. 471-474, 1999.

[14] R. M. Swanson, "Approaching the 29% limit efficiency of silicon solar cells," in *Proceedings of the 31st IEEE Photovoltaic Specialists Conference*, Orlando, USA, 2005.

[15] "Photon International," March 2009.

[16] A. Basore, "PC-1D Version 2: Enhanced Numerical Solar Cell Modeling," in *20th IEEE PVSC*, 1988 .

[17] S. M, SZE Semiconductor Devices Physics and Technology, hair Professor,NationalChiao Tung Ctniversity,: John Wiley & Sons, 1969.

[18] S. R. Eades WD, "Calculation of surface generation and recombination velocities at the Si-SiO2 interface," *Journal of Applied Physics*, vol. 58, p. 4267, 1985.

[19] F. JG., "Physical operation of back-surface-field silicon solar cells," *IEEE Transactions on Electron Devices*, vol. 24, pp. 322-325, 1977.

[20] L. C. T. M. Augustin McEvoy, Solar Cells: Materials, Manufacture and Operation, Elsevier, 2012.

[21] L. A, "Coupling light to solar cells," *Advances in Solar Energy*, vol. 8, 1993.

[22] K. M. e. al., *Optics Letters*, vol. 33, p. 2527–2529, 2008.

[23] W. E. Born M, Principles of Optics, Cambridge: Cambridge Universityty Press, 1999.

[24] FOWLES G.R., Indroduction to Modern Optics, New York: Rinehart and Winston, 1968.

[25] [Online]. Available: http://www.pveducation.org/pvcdrom/design/anti-reflection-coatings .

[26] E. W. M. Born, Principles of Optics, Cambridge,: Cambridge University Press, .

[27] W. S. Richards B, in *Proc. 28th IEEE PVSC*, 2000.

[28] J. Johnson J, in *Proc. 18th PVSC*, 1985.

[29] S. Sopori B, in *Proc 11th EC PVSEC*, 1992.

[30] S. J. e. al., in *Proc. 12th EC PVSC*, 1994.

[31] W. Ruske M, in *Proc. 20th European PVSEC*, 2005.

[32] A. Rodr’ıguez J, "Sol. Energy Mat.," *Sol. Cells*, vol. 45, pp. 241-253, 1997.

[33] G. M. Campbell P, "Light trapping properties of pyramidally textured surfaces," *Journal of Applied Physics*, vol. 62(1), p. 243 , 1987.

[34] G. M. Campbell P, "High performance light trapping textures for monocrystalline silicon solar cells.," *Solar Energy Materials and Solar Cells,* Vols. 65(1-4), pp. 369-375, 2001.

[35] S. Zhao J, "Improvements in Silicon Solar Cell Performance," in *22nd IEEE PV Specialists Conference,* 1991.

[36] G. M. Wenham SR, "Buried contact solar cell," 1988. [Online]. Available: http://www.freepatentsonline.com/4726850.html .

[37] M. Zolper JC, "16.7% efficient, laser textured, buried contact polycrystalline silicon solar cell," . *Applied Physics Letters,* vol. 55, p. 2363, 1989.

[38] M. Rover D T, "Solar cell modeling on personal computers," in *The Confernce Record of the 18th IEEE Photovoltaic Specialists Conference*, 1985.

[39] B. P. A. Clugston D A, "PC1D version 5: 32-bit solar cell modeling on personal computers," in *The Confernce Recod of the 26th IEEE Photovoltaic Specialists Confernce*, 1997.

[40] W. Basore P A, "PC-1D version 2: Enhanced numerical solar cell modeling," in *The Confernce Record of the 20the IEEE Photovoltaic Specialists Conference*, 1988.

[41] Wang J H, "Large-grain polycrystalline silicon solar cell on epitaxial thickening of AIC seed layer by Hot Wire CVD," in *IEEE Electr. Device L*, 2010.

[42] Ai B, "Study on epitaxial silicon thin film solar cells on low cost silicon ribbon substrates," in *J. Cryst Growth*, 2005.

[43] Gordon I, "8% efficient thin-film polycrystalline-silicon solar cells based on aluminium-induced crystallization and thermal CVD," in *Prog Photovoltaics*, 2007.

Annexure 01: Introduction to PC1D Simulation Software

Physics basis of device simulation by PC1D [38]

PC1D carries out device simulation by solving the following semiconductor equations for quasi-one-dimensional transport of electrons and holes in a solar cell.

$$J_n = -qn\mu_n(x)\left[\frac{\partial\psi}{\partial x} + \frac{d\Phi_n}{dx}\right] + qD_n(x)\frac{\partial n}{\partial x} \quad \text{..... (1)}$$

$$\frac{\partial n}{\partial t} = \frac{1}{q}\frac{\partial J_n}{\partial x} + G(x,t) - R(n,p) \quad \text{..... (2)}$$

$$J_p = -qp\mu_p(x)\left[\frac{\partial\psi}{\partial x} + \frac{d\Phi_p}{dx}\right] + qD_p(x)\frac{\partial p}{\partial x} \quad \text{..... (3)}$$

$$\frac{\partial p}{\partial t} = -\frac{1}{q}\frac{\partial J_p}{\partial x} + G(x,t) - R(n,p) \quad \text{..... (4)}$$

$$\frac{\partial^2\psi}{\partial x^2} = -\frac{q}{\varepsilon}\left[p - n + N_D(x) - N_A(x)\right] \quad \text{..... (5)}$$

where J_n and J_p are the electron and hole current densities, q is electron charge, n and p are the electron and hole concentrations, μ_n and μ_p are the electron and hole mobilities, ψ is the electrical potential, x is the position, t is the time, Φ_n and Φ_p are the band-gap narrowing potentials caused by heavy doping, for N-type material just the band-gap narrowing of the conduction band is considered, for P-type material just the valence band is considered, D_n and D_p are electron and hole diffusion coefficients, G is the generation rate, R is the recombination rate, N_D and N_A are the donor and acceptor doping concentrations. n, p, J_n , J_p and ψ are the functions of both the position and time. Eqs. (1) and (3) are the expressions of the electron and hole current densities, which mean that the current density at any position within a solar cell is composed of the drift current and the diffusion current (also known as the drift-diffusion approximation). Eqs. (2) and (4) come from the charge conservation law or the continuity equation. Eq. (5) is the Poisson equation for solving electrostatic field problems. By substituting eq. (1) into eq. (2), and substituting eq. (3) into eq. (4), J_n and J_p can be deleted and the five equations can be reduced to three basic equations with three unknowns (n, p and ψ).

PC1D performs solar cell modeling by solving the above three basic equations with the finite element approach. The specific process is as follows: First, the x-domain of a solar cell with thickness of L is divided (or discretized) into a finite set of M subintervals (or elements). Subsequently, in each element the three basic equations are solved. Because n, p and ψ of adjacent elements take the same values at the dividing point (or node), the three basic equations corresponding to each element are linked (or coupled) together. Within each element the generation rate is calculated according to the optical absorption properties of the material and AM1.5G spectra, and the recombination rate is obtained by summing up the contribution of the direct recombination, the Auger recombination and the Schockley-Read-Hall recombination through the band-gap states. Besides the above equations, there are three equations at each boundary that are based on the charge neutrality, the applied voltage, and the surface recombination, thus, for M elements there are a total of 3(M+l) equations for 3(M+l) unknowns. PC1D solves the 3 (M+1) fully coupled nonlinear equations with the Newton's iterative method. Given the initial conditions, PC1D first solves the fully-coupled nonlinear equations under the specified initial conditions, then based on the solutions of n, p and ψ, it constructs the new values of n, p and ψ, and substitutes them into the fully-coupled nonlinear equations again. This numerical iteration process will continue until all of the equations achieve convergency (or self-consistency), the corresponding solutions are exactly the numerical solutions of the fully-coupled nonlinear equations.

Advantages and Disadvantages of PC1D Simulation

PC1D simulation possesses the following advantages [39], [38], [40]:

- PC1D can run on an ordinary personal computer as long as the CPU has the built-in math coprocessor, without the need of using a dedicated server. PC1D 5.0 version is a 32-bit program, requiring Windows95/Windows NT or above as the operating system. Obviously, most of current personal computers can meet the needs for running PC1D.

- Use the user-friendly Windows operating interface, which is simple, direct viewing and easy to use. For example, the "parameter view" displays a parameter list of the

simulated device on the left, and a schematic diagram of the device on the right, providing user a real-time visual feedback when parameters are changed.

- PC1D can output interactive graphs of various physical quantities, such as the curves of carrier concentration, current density, generation and recombination rate, electric potential, electrical field strength as function of positions, illuminated *I-V* characteristic curve, power curve, quantum efficiency & reflectance curve, etc. This is particularly helpful for intensively analyzing the performance of a solar cell.

- More powerful and flexible simulation capability and wider applicability. A solar cell with up to five regions can be modeled, and each region can be of different materials, with its own parameters. The internal model allows for two diffusions at each surface, and each diffusion can take the form of uniform distribution, or exponential distribution, or Gaussian distribution, or Erfc distribution or directly use an external file including the experimental data. Different light trapping structures such as textured front or rear surface, single or multiple antireflection layers can be modeled. Furthermore, the internal optical reflectance at each surface can be set as specular or diffuse reflectance and given different values. PC1D also allow user to directly use an external file containing the reflectance data. Up to four internal shunt elements like diodes or parallel resistors can be activated in circuit connection option.

- More accurate performance prediction results and faster convergence velocity. After more than 20 years continuous improvement on the physical models, the material characteristic parameters and the numerical simulation methods, PC1D can predict the performance of a solar cell fast and accurately, especially for simulation of a crystalline silicon solar cell, it can obtain very high accuracy and reliability.

The major shortcomings of PC1D are as follows:

- PC1D does not include the characteristic parameters and physical models of hydrogenated amorphous silicon material, thus PC1D cannot simulate a solar cell containing the hydrogenated amorphous silicon.

- PC1D is a 1D simulation software such that it cannot perform precise numerical simulation on a solar cell with two-or three-dimensional structure inhomogeneity such as the BPC (backside point contact) and the EWT (emitter-wrap-through) solar cell. Of course, “equivalent structure” or “effective parameter” method can be used to convert them into 1D devices, and then use PC1D to perform numerical simulation.